Diverse states and stimuli tune olfactory receptor expression levels to modulate food-seeking behavior

Ian G. McLachlan[1], Talya S. Kramer[1,2,*], Malvika Dua[1,*], Elizabeth M. DiLoreto[3], Matthew A. Gomes[1], Ugur Dag[1], Jagan Srinivasan[3], Steven W. Flavell[1,**]

[1]Picower Institute for Learning and Memory, Department of Brain and Cognitive Sciences, Massachusetts Institute of Technology, Cambridge, MA, USA
[2]MIT Biology Graduate Program, Massachusetts Institute of Technology, Cambridge, MA, USA
[3]Department of Biology and Biotechnology, Worcester Polytechnic Institute, Worcester, MA, USA
[*]These authors contributed equally
[**]Correspondence: flavell@mit.edu

ABSTRACT

Animals must weigh competing needs and states to generate adaptive behavioral responses to the environment. Sensorimotor circuits are thus tasked with integrating diverse external and internal cues relevant to these needs to generate context-appropriate behaviors. However, the mechanisms that underlie this integration are largely unknown. Here, we show that a wide range of states and stimuli converge upon a single *C. elegans* olfactory neuron to modulate food-seeking behavior. Using an unbiased ribotagging approach, we find that the expression of olfactory receptor genes in the AWA olfactory neuron is influenced by a wide array of states and stimuli, including feeding state, physiological stress, and recent sensory cues. We identify odorants that activate these state-dependent olfactory receptors and show that altered expression of these receptors influences food-seeking and foraging. Further, we dissect the molecular and neural circuit pathways through which external sensory information and internal nutritional state are integrated by AWA. This reveals a modular organization in which sensory and state-related signals arising from different cell types in the body converge on AWA and independently control chemoreceptor expression. The synthesis of these signals by AWA allows animals to generate sensorimotor responses that reflect the animal's overall state. Our findings suggest a general model in which sensory- and state-dependent transcriptional changes at the sensory periphery modulate animals' sensorimotor responses to meet their ongoing needs and states.

INTRODUCTION

To thrive in a dynamic environment, animals must continuously integrate their perception of the outside world with their internal needs and experiences. Thus, virtually all animals exhibit long-lasting internal states that reflect their physiology and experience and in turn influence sensorimotor processing. For example, an animal's nervous system might respond to the recent absence of food sensory cues and a metabolic energy deficit by generating a neural representation of hunger, which in turn alters a wide range of feeding-related behaviors. In real-world environments, an animal's nervous system is responsible for evaluating a number of needs simultaneously to prioritize behavioral outputs – such as avoiding predation while seeking food –

to ensure that all needs are ultimately met. The biological underpinnings of these complex, integrated state-dependent behavioral changes remain poorly understood.

Decades of experimental work has identified neuronal populations that can induce internal states (Flavell et al., 2022). For example, NPY/AgRP neurons in the hypothalamus drive behavioral changes typical of hunger (Aponte et al., 2011; Clark et al., 1984; Krashes et al., 2011; Luquet et al., 2005), neurons in the lamina terminalis drive those typical of thirst (Johnson and Gross, 1993; Oka et al., 2015), and subpopulations of neurons in the ventromedial hypothalamus drive aggressive behaviors (Kruk et al., 1983; Lin et al., 2011). Likewise, P1 interneurons in *Drosophila* can trigger a state of social arousal (Hindmarsh Sten et al., 2021; Hoopfer et al., 2015), and serotonergic NSM neurons in *C. elegans* can trigger dwelling states during foraging (Flavell et al., 2013; Ji et al., 2021; Rhoades et al., 2019; Sawin et al., 2000). These devoted cell populations appear to respond to state-relevant inputs and elicit a suite of behavioral changes that comprise the state. However, animals can exhibit more than one state at a time, like hunger, stress, or aggression. Therefore, the sensorimotor pathways that implement specific motivated behaviors, such as approach or avoidance of a sensory cue, must integrate information about multiple states to adaptively control behavior. Previous work has revealed that neuromodulators and hormones can convey state information to sensory circuits to allow for state-specific sensorimotor processing (Horio and Liberles, 2021; Inagaki et al., 2014; Jourjine et al., 2016; Ko et al., 2015; Root et al., 2011; Sayin et al., 2019; Takeishi et al., 2020; Yapici et al., 2016), but how diverse state-related inputs are integrated by these circuits remains unclear.

The nematode *C. elegans*, whose nervous system consists of 302 defined neurons with known connectivity (White et al., 1986; Witvliet et al., 2021), exhibits a wide range of state-dependent behavioral changes (Flavell et al., 2020). Food deprivation leads to a suite of behavior changes, such as exaggerated dwelling and increased feeding rates upon encountering food (Avery and Horvitz, 1990; Ben Arous et al., 2009; Sawin et al., 2000; Shtonda and Avery, 2006); harmful stimuli can trigger states of generalized aversion or stress-induced sleep (Chew et al., 2018; Hill et al., 2014); and infection by a bacterial pathogen can trigger bacterial avoidance and changes in bacterial preference (Kim and Flavell, 2020; Meisel et al., 2014; Zhang et al., 2005). The *C. elegans* neuromodulatory systems (Bentley et al., 2016) allow these states to influence sensorimotor circuits: the effects of hunger are mediated by amines and insulin signaling (Ghosh et al., 2016; Skora et al., 2018; Takeishi et al., 2020); stressors induce the release of tyramine and neuropeptides that alter behavior (De Rosa et al., 2019; Nath et al., 2016; Nelson et al., 2014); and bacterial infection induces the release of *daf-7*/TGFβ, which promotes bacterial lawn leaving (Meisel et al., 2014). The well-defined behavioral states of *C. elegans*, together with its relatively simple sensorimotor circuits, make it an attractive system to decipher how animals generate sensorimotor behaviors that reflect an integration of their states.

Sensorimotor processing in *C. elegans* originates in primary sensory neurons that detect odorants, tastants, touch, temperature, and more (Iliff and Xu, 2020). Each of the 16 chemosensory neuron pairs expresses a multitude of chemoreceptors, which are predominantly G-protein coupled receptors (GPCRs) (Ferkey et al., 2021). Detection of odorants or tastants evokes changes in sensory neuron activity that are transmitted to downstream interneurons and motor circuits (Chalasani et al., 2007; Suzuki et al., 2008). Several chemosensory neurons, such as AWA and AWC, primarily detect appetitive cues, while others, including ASH, detect aversive cues. However, chemosensory processing can be modulated by internal state and

learning (Flavell and Gordus, 2022). For example, insulin signaling drives a hunger-dependent switch in thermotaxis behavior by modulating the AWC sensory neuron (Takeishi et al., 2020). Associative learning can drive changes in salt or temperature preference by altering presynaptic release from the ASE and AFD neurons that detect these respective stimuli (Hawk et al., 2018; Ohno et al., 2017). Neuromodulation of sensory interneurons also impacts sensory processing (Chen et al., 2017). In addition, internal states have been shown in some cases to modulate gene expression in chemosensory neurons. Starvation alters the expression of the *str-234* chemoreceptor in ADL (Gruner et al., 2014) and the diacetyl receptor *odr-10* in AWA (Ryan et al., 2014; Wexler et al., 2020). Infection and starvation can modulate *daf-7*/TGFβ expression in ASJ (Hilbert and Kim, 2017). This work suggests that changes in chemosensory neuron gene expression are well-poised to underlie state-dependent changes in sensorimotor processing, and likewise represent a plausible locus of state integration.

Here, we show that the olfactory neuron AWA integrates multiple streams of information to regulate chemoreceptor expression and dictate state-dependent food-seeking behavior. State-dependent ribotagging reveals that the expression of chemoreceptor genes is disproportionately elevated in AWA following food deprivation. We find that AWA chemoreceptor expression is controlled by both the sensory and metabolic components of food, as well as physiological stress. The state-dependent chemoreceptor *str-44* confers responsiveness to the putative food odors butyl acetate and propyl acetate and promotes starved-like foraging behaviors when expressed at high levels in AWA. Further, we delineate the neural and molecular pathways that underlie convergent signaling to AWA, identifying signaling pathways from other sensory neurons to AWA, a gut-to-brain metabolic pathway that signals to AWA, and a physiological stress pathway. These pathways act in a modular fashion and each contribute independently to the levels of AWA chemoreceptor expression. Our results reveal how diverse external and internal cues -- nutritional state, stress, and sensory environment -- converge at a single node in the *C. elegans* nervous system to allow for an adaptive sensorimotor response that reflects a complete integration of the animal's states.

RESULTS

Diverse external and internal cues regulate chemoreceptor expression in the AWA olfactory neuron

As an unbiased approach to identify neural mechanisms that underlie state-dependent behavioral changes, we performed molecular profiling of *C. elegans* neurons in well-fed versus food-deprived animals. We selected three hours of food deprivation as our time point because it is sufficient to induce many feeding-related behavioral changes, including alterations in food approach, encounter, and exploitation (Rhoades et al., 2019), while remaining a relatively mild metabolic insult. To obtain a "snapshot" of gene expression while animals were in a specific state, we used pan-neural ribotagging. This method permits cell-specific purification of actively-translating mRNAs from animals that are flash frozen within minutes after removal from plates. We expressed an HA-tagged ribosomal subunit in all neurons, purified the tagged mRNA-ribosome complexes from fed and three-hour fasted adult animals, and sequenced the isolated mRNAs and whole-animal input RNA (see Methods)(McLachlan and Flavell, 2019). High-depth mRNA sequencing of ribotag samples allowed us to detect mRNAs that were being actively translated in as few as a single pair of neurons. We performed three independent

134 biological replicates (Figure 1—figure supplement 1A) and confirmed the enrichment of pan-
135 neural mRNAs in ribotag samples (Figure 1—figure supplement 1B). We examined the genes
136 whose expression was most dramatically altered by fasting: 802 genes were increased >4-fold in
137 the fasted condition compared to the fed condition, while 647 were decreased >4-fold (Figure
138 1A; Supplementary File 1). Strikingly, chemosensory GPCRs were significantly overrepresented
139 among the upregulated genes (133/802 upregulated genes, $p < 0.001$, Fisher Exact Test,
140 compared to ~8.5% overall prevalence in the genome; Figure 1—figure supplement 1C). These
141 results suggest that food deprivation causes an upregulation of chemosensory GPCRs in *C.*
142 *elegans* neurons.

143 As a first step to identify the neurons where the fasting-induced chemosensory GPCRs are
144 expressed, we examined the site(s) of expression of these 133 genes in publicly-available single-
145 cell sequencing data (Taylor et al., 2021). We found that these chemoreceptors are distributed
146 across all neurons in the amphid sense organ, suggesting that fasting induces broad changes in
147 olfactory coding by sensory neurons (Figure 1B, grey bars). To determine if any sensory neurons
148 exhibit a disproportionate change in chemoreceptor expression profile after fasting, we
149 normalized the counts of upregulated receptors to the overall number of chemosensory GPCRs
150 expressed by each neuron. We found that the AWA olfactory neuron expressed a significantly
151 greater proportional enrichment of upregulated GPCRs than expected if chemoreceptors genes
152 were upregulated uniformly across neuron types (24/133 chemoreceptors, Figure 1B, green bars;
153 Figure 1—figure supplement 1D). This suggests that AWA chemoreceptor expression levels are
154 particularly sensitive to food deprivation.

155 To directly monitor the sites of chemoreceptor expression, we generated *in vivo* transcriptional
156 reporters by inserting a t2a-mNeonGreen fluorescent reporter at the C-termini of several
157 chemoreceptor genes via CRISPR-based gene editing (Figure 1C). As our ribotagging results
158 suggested that these genes were upregulated after fasting, we compared mNeonGreen
159 fluorescence for each of these chemoreceptors in fed and three hour fasted animals. For the *str-*
160 *44* and *srd-28* chemoreceptor genes, we observed very little fluorescence in fed animals, but a
161 significant increase specifically in AWA in fasted animals (Figure 1D; confirmation by co-
162 expression of an AWA marker in Figure 1—figure supplement 1E). As a point of comparison,
163 expression of a mNeonGreen reporter inserted into the well-characterized AWA-specific
164 chemoreceptor *odr-10* was detectable in fed animals and displayed only a small, non-significant
165 increase after fasting, consistent with the fact that it was only mildly upregulated by fasting in
166 our ribotagging data (Figure 1D). As a negative control, we generated a reporter for the serotonin
167 receptor *ser-7*, a GPCR in a different gene family whose expression was not altered in our
168 ribotagging data, and observed that its expression was not affected by fasting. This suggests that
169 the t2a-mNeonGreen transgene does not aberrantly confer fasting-dependent regulation. Overall,
170 these reporter gene results provide a close match to our ribotagging data. These data suggest that
171 fasting causes an upregulation of chemoreceptors in the AWA olfactory neuron.

172 Because the ~5-fold increase in *str-44* expression upon food deprivation was particularly reliable
173 and we were able to identify odorants that activate STR-44 (see below), we focused our
174 experiments on this chemosensory GPCR. Depriving animals of their bacterial food for three
175 hours impacts them in two ways: it leads to a change in metabolic state due to decreased
176 ingestion and it causes a change in sensory experience due to the removal of food sensory
177 cues. To determine which of these effects influence *str-44* expression, we exposed animals to

178 food cues under conditions where they were unable to ingest the food. First, we exposed
179 animals to bacteria treated with aztreonam, which inhibits cell division and renders the
180 bacteria too large to consume. This manipulation led to a level of *str-44* expression that was
181 intermediate to well-fed and fasted animals (Figure 1E). This suggests that the ingestion of
182 bacteria is necessary to fully suppress *str-44* expression, but also that non-nutritive
183 components of the bacteria, such as volatile odorants, can partially suppress *str-44*
184 expression. However, aztreonam treatment may also alter mechanosensory or chemical
185 properties of the bacterial lawn, and therefore the sensory experience of the animal is not
186 strictly identical to the untreated lawn. Therefore, we also used a second approach in which
187 we exposed animals to food that was placed on the lid of the plate, rendering it inaccessible
188 to the animal. As expected, this manipulation also produced a level of *str-44* expression that
189 was intermediate to well-fed and fasted animals (Figure 1E). Together, these experiments
190 suggest that both food sensory cues and the actual ingestion of food act to suppress olfactory
191 receptor expression in AWA (Figure 1E).

192 In the wild, *C. elegans* interact with and ingest diverse microbial species (Samuel et al., 2016)
193 that differ both in the odors that they emit and their metabolic contents. Given that AWA
194 chemoreceptor expression is regulated by both sensory and metabolic cues, we hypothesized that
195 AWA chemoreceptor expression might be modulated not just by the presence or absence of
196 bacteria, but also by exposure to different bacterial food sources. To test this, after raising
197 animals on the standard laboratory diet of *E. coli* (OP50), we transferred them to plates where
198 they were able to consume different bacterial species for three hours. We sampled representative
199 bacterial strains from five different genuses: *Stenotrophomonas* (JUb19), *Pantoea* (BIGb0393),
200 *Comamonas* (DA1877), *Pseudomonas* (PA14), and *Ochrobactrum* (MYb71). Indeed, the levels
201 of *str-44*::mNeonGreen reporter expression were increased significantly compared to *E. coli*
202 OP50 controls when animals were exposed to *Comamonas* DA1877 or *Pseudomonas* PA14
203 (Figure 1F), two species that are naively attractive to *C. elegans* (Shtonda and Avery, 2006;
204 Zhang et al., 2005). These changes could be due to differences in sensory cues and/or metabolic
205 contents of these bacteria. By comparing the above results to conditions where DA1877 and
206 PA14 were inaccessible on the lid of the plate, we found that the odors had differential effects on
207 chemoreceptor expression. Relative to fasted controls, PA14 odor increased *str-44* reporter
208 expression, whereas DA1877 odor suppressed *str-44* expression. Thus, the effect of PA14
209 exposure may be driven by volatile odors while the effect of DA1877 exposure may be driven by
210 ingestion and/or physical contact with the bacteria (Figure 1—figure supplement 1F). Together,
211 these data suggest that exposure to different bacterial odors and metabolic contents impacts the
212 expression of AWA olfactory receptors.

213 We next sought to determine whether AWA chemoreceptor expression is exclusively controlled
214 by feeding-related signals or, alternatively, whether it is impacted by a broader set of external
215 and internal cues. Thus, we also examined whether the addition of aversive/stressful stimuli
216 influenced *str-44* expression. We chose to use a mild osmotic stressor (300 mOsm growth media,
217 versus 150 mOsm in normal media) that modulates *C. elegans* behavior, but does not adversely
218 impact animal growth rates or viability (Yu et al., 2017; Zhang et al., 2008). We found that
219 animals fasted in the presence of this physiological stressor displayed *str-44* expression that was
220 significantly suppressed relative to fasted controls (Figure 1G). However, the *ser-*
221 *7*::mNeonGreen control reporter was unaffected by this mild osmotic stressor, indicating that
222 these effects are not due to generic downregulation of GPCRs or diminished expression of

223 mNeonGreen in response to osmotic stress (Figure 1G). Taken together, these results suggest
224 that rather than relying on food-related signals alone, diverse external and internal cues converge
225 on AWA to coordinately regulate the expression of the *str-44* chemoreceptor. Given that our
226 ribotagging analysis identified >20 putative AWA chemoreceptors impacted by fasting, it is
227 possible that many AWA chemoreceptors display similar gene expression changes in response to
228 various states.

229 **The state-dependent chemoreceptor STR-44 acts in AWA to detect the attractive odors**
230 **propyl acetate and butyl acetate**

231 We next sought to understand how convergent signaling onto AWA might allow animals to
232 generate context-appropriate sensorimotor responses. Therefore, we focused on examining how
233 the state-dependent AWA chemoreceptors influence *C. elegans* sensorimotor behaviors. AWA is
234 an olfactory neuron that drives attraction to volatile odors (Ferkey et al., 2021). To identify odors
235 that activate the state-dependent chemoreceptors, we generated strains that ectopically expressed
236 either *str-44* or *srd-28* in the nociceptive sensory neuron ASH and asked whether this could
237 confer repulsion to odors previously shown to activate AWA (Larsch et al., 2013). To reduce
238 native responses to these odors, we performed these experiments in a genetic background with an
239 *odr-7* mutation, which inactivates AWA, and a *tax-4* mutation, which prevents sensory
240 transduction in other olfactory neurons. We tested olfactory behavior using a chemotaxis assay,
241 measuring movement towards or away from each of the tested odors. Due to their genetic
242 background, we predicted that these animals would generally have neutral responses to the tested
243 odors. However, if an odor were a ligand for the *str-44* or *srd-28* receptor, then expression of that
244 receptor in ASH should drive a repulsive response to the odor. As expected, the ASH::*str-44* and
245 ASH::*srd-28* strains had neutral responses to most tested odors, indistinguishable from the *odr-*
246 *7;tax-4* control strain. However, the ASH::*str-44* strain was significantly repulsed by two
247 structurally similar esters, propyl acetate and butyl acetate, suggesting that *str-44* chemoreceptor
248 expression in ASH is sufficient to confer detection of these two odors (Figure 2A). The
249 ASH::*srd-28* strain did not generate any significant responses to the odors tested, suggesting that
250 *srd-28* may detect other odors that we did not test here (Figure 2A). These data suggest that the
251 odors propyl and butyl acetate are detected by the *str-44* olfactory receptor.

252 We next examined how wild-type animals respond to propyl and butyl acetate. Wild-type
253 animals were strongly attracted to both of these odors. However, *odr-7* mutants lacking AWA
254 had significantly decreased responses to these odors, indicating that AWA is necessary for
255 navigation to propyl and butyl acetate (Figure 2B). Based on these results, we examined whether
256 AWA calcium responses to butyl and propyl acetate were state-dependent. We measured AWA
257 GCaMP signals while delivering 10s pulses of odor via microfluidic delivery. Consistent with
258 prior work (Larsch et al., 2013), AWA calcium levels increased in response to the addition of
259 either butyl or propyl acetate (Figures 2C, 2D, and Figure 2—figure supplement 1). Notably, we
260 found that fasted animals exhibited significantly increased responses to these odors compared to
261 well-fed animals (Figures 2C, 2D, and Figure 2—figure supplement 1). Thus, AWA calcium
262 responses to the cues detected by the *str-44* chemoreceptor are potentiated in fasted animals,
263 when *str-44* is expressed at high levels. Because AWA can detect butyl and propyl acetate in the
264 fed state, when *str-44* levels are often undetectable, we expect that multiple chemoreceptors
265 contribute to detection of these odorants. In addition, we have not ruled out that other fasting-

266 upregulated chemoreceptors in AWA (Figure 1B) may also contribute to the fasting-induced
267 potentiation of the response to propyl and butyl acetate.

268 **STR-44 expression drives state-dependent enhancement of behavioral preference for the**
269 **attractive odor butyl acetate**

270 We hypothesized that animals' behavioral responses to *str-44*-sensed odors would be modulated
271 by the states and stimuli that alter *str-44* expression levels, and that direct perturbations of *str-44*
272 expression would also impact behavior. To test this, we used a modified food choice assay
273 (Worthy et al., 2018) in which animals choose between two small and equidistant lawns of *E.*
274 *coli* OP50 bacterial food. We placed a spot of butyl acetate adjacent to one lawn, and as a
275 control, placed a spot of ethanol adjacent to the other lawn (Figure 2E). We chose to use this
276 assay instead of chemotaxis because fasted animals display generically reduced movement in the
277 presence of single odorants but display robust movement in food choice assays. At high
278 concentrations of odor, both fed and fasted animals were attracted to the food lawn with butyl
279 acetate (Figure 2F). However, at lower odor concentrations, fasted animals were significantly
280 more likely than fed animals to approach the food lawn with butyl acetate (Figure 2F). This
281 suggests that fasted animals display increased sensitivity to the attractive odor butyl acetate,
282 consistent with the increased expression of the butyl acetate receptor *str-44* in fasted animals. To
283 test whether increased expression of *str-44* could directly drive increased sensitivity to butyl
284 acetate, we generated a strain that overexpresses *str-44* under a constitutive AWA promoter,
285 driving overexpression in both fed and fasted animals. Indeed, well-fed animals from this strain
286 were significantly more likely to approach the butyl acetate food lawn compared to well-fed
287 wild-type animals, phenocopying the fasted state (Figure 2G). We also tested whether the
288 fasting-induced increase in butyl acetate sensitivity requires AWA and/or *str-44*. *odr-7* mutants
289 lacking a functional AWA did not display a fasting-induced increase in butyl acetate attraction,
290 suggesting that AWA is required for this effect (Figure 2G). In addition, *str-44;srd-28* double
291 mutants displayed an attenuated behavioral response where their attraction to the butyl acetate
292 lawn was similar in fed and fasted conditions, suggesting that *str-44* and/or *srd-28* are necessary
293 for normal fasting-induced enhancement of butyl acetate preference (Figure 2—figure
294 supplement 1D). Together, these results indicate that *C. elegans* displays an AWA-dependent
295 increase in sensitivity to butyl acetate upon fasting and that expression of the fasting-upregulated
296 AWA chemoreceptor *str-44* can drive increased sensitivity to this odor.

297 We next examined whether other manipulations that increase or decrease *str-44* expression could
298 likewise modify butyl acetate sensitivity. Since the presence of mild osmotic stress blocks the
299 upregulation of *str-44* in AWA during fasting, we examined whether this manipulation also
300 blocks the fasting-induced increase in butyl acetate sensitivity. Indeed, when we tested fasted
301 animals undergoing osmotic stress, they were no more likely to approach the butyl acetate food
302 lawn than well-fed controls (Figure 2G). Together with the direct manipulations of *str-44* levels
303 described above, these results suggest that the level of *str-44* expression in AWA, which is set
304 via the integration of multiple states, drives butyl acetate sensitivity. More broadly, these results
305 are consistent with the notion that integrated state-dependent changes in the expression of *str-44*
306 and potentially other chemoreceptors may alter sensory responses to specific odors, allowing
307 animals to modulate their navigation based on the sum of their recent experience and physiology.

308 **AWA responses to food are influenced by internal state, and the state-dependent olfactory**
309 **receptors drive enhanced responses to food**

310 In natural environments, *C. elegans* encounter complex mixtures of olfactory stimuli rather
311 than monomolecular odorants, so we next asked whether the response of AWA to bacterial
312 odors is influenced by the same states that modify AWA chemoreceptor expression. Previous
313 studies have shown that AWA responds to bacterial volatiles (Zaslaver et al., 2015), which are
314 complex mixtures of heterogeneous odorants, including esters like butyl and propyl acetate. To
315 examine state-dependent AWA calcium responses to food odor gradients, we performed AWA
316 GCaMP imaging in freely-moving fed or fasted animals as they navigated towards a lawn of *E.*
317 *coli* OP50 food (Figure 3A). Across conditions, AWA displayed notable calcium peaks as
318 animals navigated towards the food lawn (Figure 3B). These responses mostly occurred when
319 animals were in close proximity to the food lawn and when they were moving up the odor
320 gradient towards the food. The amplitudes and durations of these peaks were significantly
321 increased in fasted animals compared to fed animals (Figures 3C and Figure 3—figure
322 supplement 1A). This resulted in a significant difference in overall AWA activity between fed
323 and fasted animals that was maximally apparent shortly before lawn encounter (Figure 3D). The
324 fasting-induced increase in AWA food responses was attenuated by exposing animals to mild
325 osmotic stress during fasting (Figures 3C and 3D), matching the above results that this stressor
326 suppresses the fasting-induced increase in *str-44* expression. These results indicate that AWA
327 responses to bacterial food odor gradients are influenced by an integrated internal state including
328 fasting and stress.

329 These experiments suggested that changes in AWA chemoreceptor expression might influence
330 food-driven behaviors, much like they influence butyl acetate odor preference. Thus, we utilized
331 an assay of bacterial food exploration during foraging. Fasted animals reduce their locomotion
332 on a food lawn compared to fed animals, reflecting increased exploitation of a food source after
333 fasting (Ben Arous et al., 2009; Shtonda and Avery, 2006). We hypothesized that fed animals
334 that overexpress *str-44* in AWA would behave as if they were fasted, much like in the above
335 food choice experiments. Indeed, we observed that overexpressing *str-44* and *srd-28* in AWA led
336 to a marked decrease in exploration in the fed state, mimicking the behavior of fasted wild-type
337 animals (Figure 3E). This effect on movement was only observed in the presence of bacterial
338 food, as the same overexpression strain displayed wild-type speed in the absence of food (Figure
339 3—figure supplement 1B). Thus, increasing *str-44* and *srd-28* expression in AWA is sufficient to
340 alter food-driven changes in locomotion, partially mimicking the behavior of fasted animals.
341 Taken together with the above results, these data suggest that AWA calcium responses to
342 bacterial food are enhanced by fasting, and that increased expression of the fasting-induced
343 olfactory receptor *str-44* results in fasted-like behavioral responses to food. Overall, the
344 behavioral studies that we have carried out indicate that state-dependent modulation of AWA
345 chemoreceptor expression, in particular *str-44* expression, alters the animal's sensorimotor
346 behaviors related to food navigation and foraging.

347 **Signaling from a set of food sensory neurons to AWA regulates *str-44* expression**

348 We next sought to understand the mechanisms by which AWA integrates diverse external and
349 internal cues to influence sensorimotor behaviors. Our overall approach was to first determine
350 the molecular and neural pathways that convey each sensory stimulus or state to AWA and then

351 examine how they interact. We first examined how food sensory cues influence AWA olfactory
352 receptor expression. We examined *str-44*::mNeonGreen reporter fluorescence in *tax-4* mutants
353 that have defective sensory transduction in many food-responsive sensory neurons (Ferkey et al.,
354 2021). Importantly, AWA sensory transduction does not require *tax-4* (Ferkey et al., 2021).
355 Well-fed *tax-4* mutants exhibited a striking increase in *str-44* expression compared to wild-type
356 controls, with expression levels even greater than wild-type fasted animals (Figure 4A).
357 Correspondingly, well-fed *tax-4* mutants exhibited increased attraction to the STR-44-sensed
358 odor butyl acetate (Figure 4F). A potential concern is that an increase in *str-44* expression may
359 occur if a mutation reduces food intake; however, we found that *tax-4* animals displayed normal
360 feeding rates (Figure 4—figure supplement 1A shows normal feeding rates for *tax-4* and all other
361 mutants/transgenics with elevated *str-44* expression in fed animals). This phenotype could be
362 rescued by expressing the *tax-4* cDNA under its own promoter (Figure 4A). This suggests that
363 impaired sensory transduction in one or more *tax-4*-expressing sensory neuron increases *str-44*
364 expression in the AWA sensory neuron. In addition, we found that *tax-4* mutants also have
365 elevated expression of another AWA chemoreceptor, *srd-28* (Figure 4—figure supplement 1G).
366 Thus, crosstalk between sensory neurons regulates AWA chemoreceptor expression. Such
367 crosstalk could occur either through direct synaptic communication between sensory neurons,
368 extrasynaptic neuromodulation, or feedback through bidirectional interneurons.

369 We next determined which *tax-4*-expressing neurons functionally regulate *str-44* expression. To
370 do so, we impaired the function of these neurons individually and examined the effect on *str-*
371 *44*::mNeonGreen reporter fluorescence. Chemogenetic silencing of AWB, BAG, ASI,
372 AQR/PQR/URX, or ASK via a histamine-gated chloride channel (HisCl)(Pokala et al., 2014) led
373 to a significant increase in *str-44* expression in well-fed animals, whereas ASJ silencing had no
374 effect (Figure 4B; feeding controls in Figure 4—figure supplement 1B; histamine controls in
375 Figure 4—figure supplement 1C). In fasted animals, chemogenetic silencing did not further
376 increase *str-44* expression except in ASK, and silencing of ASI reduced *str-44* expression
377 relative to fasted controls (Figure 4—figure supplement 1D-E), which may reflect distinct
378 requirements for ASI in fed versus fasted states. Genetic ablation of AWC and ASE via *ceh-36*
379 mutation also had no effect on *str-44* expression in fed animals (Figure 4—figure supplement 1F;
380 see also for additional mutants and transgenics that corroborate these findings). These data
381 indicate that a defined set of *tax-4*-expressing neurons inhibit AWA *str-44* expression in well-fed
382 animals. Notably, each of the neurons that inhibit *str-44* expression have been previously shown
383 to detect food sensory cues (Ferkey et al., 2021). Taken together, these data suggest that food
384 sensory cues are detected by AWB, BAG, ASI, AQR/PQR/URX, and ASK, which signal to
385 AWA to inhibit *str-44* expression while animals are feeding.

386 In principle, these food sensory neurons could signal to AWA through neuropeptide release
387 and/or synaptic outputs onto downstream circuit components that in turn synapse onto AWA. We
388 separately examined these possibilities. Among the neuropeptidergic pathways, the insulin/IGF-1
389 signaling pathway (IIS) has been most prominently linked to feeding state, and several of the
390 food sensory neurons that regulate *str-44*, such as ASI, release insulin peptides. Insulin acts
391 primarily through the *daf-2* insulin receptor (Murphy and Hu, 2013). Activation of *daf-2* alters
392 gene expression by inhibiting the *daf-16*/FOXO transcription factor, which is also a target of
393 other cellular signaling pathways (Landis and Murphy, 2010). Loss of the *daf-2* insulin receptor
394 also caused a strong de-repression of *str-44* and a corresponding increase in butyl acetate
395 attraction (Figures 4C and 4F). Conversely, *daf-16* mutants showed nearly abolished *str-44*

396 expression (Figure 4C). The *daf-2* insulin receptor and *daf-16*/FOXO are broadly expressed, so
397 we next examined where they function. Expression of the *daf-2* cDNA specifically in AWA
398 rescued *str-44* expression to wild-type levels (Figure 4C). Expression of the *daf-16a* cDNA
399 specifically in AWA rescued *str-44* expression, albeit not completely; expression of this cDNA
400 in all tissues yielded the same result, suggesting that additional isoforms of *daf-16* are required
401 (Figure 4C). Finally, we determined that *daf-2* and *daf-16* mutants respectively increase and
402 decrease *srd-28* expression in AWA (Figure 4—figure supplement 1H). Together, these results
403 suggest that *daf-2* and *daf-16* act in AWA to regulate olfactory receptor expression.

404 We also examined whether other neuropeptide signaling pathways could influence *str-44*
405 expression. Most neuropeptides act on GPCRs that couple to the G proteins Gao/*goa-1*, Gas/*gsa-*
406 *1*, or Gaq/*egl-30*, which are all natively expressed in AWA (Taylor et al., 2021). Thus, we
407 mimicked the activation of neuropeptide receptors in AWA via AWA-specific expression of
408 constitutively-active versions of these G proteins and examined the impact on *str-44* expression.
409 AWA-specific expression of Gao/*goa-1(gf)* or *acy-1(gf),* a key Gas/*gsa-1* effector, drove a robust
410 increase in *str-44* expression, whereas expression of Gaq/*egl-30(gf)* had only a mild effect
411 (Figure 4—figure supplement 2A). This suggests that activation of specific G protein signaling
412 pathways in AWA can influence *str-44* expression and raises the possibility that additional
413 neuropeptides that act through these canonical pathways regulate *str-44*.

414 We next tested whether sensory habituation in AWA is a suitable explanation for the odor-driven
415 reduction in *str-44* expression. We exposed wild-type animals to the *str-44* odorants butyl acetate
416 or propyl acetate during three hours of either feeding or fasting and measured *str-44* expression.
417 If habituation explains this effect, we would expect that exposure to these odorants would reduce
418 *str-44* expression in fasted animals. However, we observed no differences between odor-exposed
419 animals and controls (Figure 4—figure supplement 2B), suggesting that *str-44* expression levels
420 are not modulated by activation of the STR-44 receptor.

421 Finally, we examined whether the food sensory neurons could feasibly signal to AWA via action
422 on downstream neural circuits. AWA receives strong synaptic input (>3 synapses) from three
423 neurons in the *C. elegans* wiring diagram: ASI, one of the food sensory neurons that represses
424 *str-44* expression; and AIA and AIY, which are second-order neurons in the chemosensory
425 circuit that together receive synaptic inputs from all five of the food sensory neurons that inhibit
426 *str-44* (White et al., 1986; Witvliet et al., 2021). To test whether AIA and AIY are required for
427 proper *str-44* regulation, we inactivated these cells via expression of tetanus toxin light chain
428 (TeTx). Synaptic silencing of AIA led to a significant decrease in *str-44* expression in fasted
429 animals, whereas synaptic silencing of AIY had no effect (Figure 4D). In addition, direct
430 chemogenetic silencing of AWA also inhibited *str-44* expression, suggesting that modulating
431 AWA activity itself can influence *str-44* expression (Figure 4E; histamine controls in Figure 4—
432 figure supplement 2C). To distinguish between a direct effect of AWA activity on intracellular
433 gene expression and a feedback effect of reduced AWA synaptic transmission, we also measured
434 *str-44* expression in animals expressing TeTx in AWA. Inhibition of synaptic release from AWA
435 had no effect on *str-44* expression, suggesting that AWA activity autonomously controls AWA
436 chemoreceptor levels (Figure 4—figure supplement 2D). These data suggest that a sensory
437 circuit consisting of several food sensory neurons and their downstream synaptic target AIA
438 regulates AWA chemoreceptor expression. Taken together with the above results, these data
439 reveal that several signaling mechanisms – insulin signaling, G-protein signaling, and activity-

440 dependent signaling – allow a defined set of food sensory neurons to regulate olfactory receptor
441 expression in AWA (Figure 4G).

442 ***rict-1*/TORC2 signaling in the intestine signals to AWA to underlie metabolic regulation of**
443 **AWA chemoreceptor expression**

444 In addition to food sensory signals, our experiments suggest that the actual ingestion of food
445 influences chemoreceptor expression in AWA (Figures 1E and 1F). We therefore sought to
446 identify pathways that link physiological fasting to *str-44* expression levels in AWA.
447 Monoaminergic neuromodulators including serotonin and octopamine can act as internal signals
448 of food availability (Rhoades et al., 2019; Sawin et al., 2000; Srinivasan et al., 2008), so we
449 examined *cat-1*/VMAT mutants, which are defective in the release of these neuromodulators.
450 However, these mutants displayed normal *str-44* expression in fed and fasted states (Figure 5A).
451 Likewise, *pdfr-1* animals lacking PDF neuropeptide signaling, which acts in opposition to
452 serotonin (Flavell et al., 2013), displayed normal *str-44* expression (Figure 5A). We next
453 examined whether changes in internal fat stores, which can impact nervous system function
454 (Witham et al., 2016), influence *str-44* expression. However, mutations that disrupt the ability of
455 the animal to store fat (*mxl-3,* MAX transcription factor) or metabolize triglycerides (*atgl-1*,
456 adipose triglyceride lipase) did not alter *str-44* expression (Figure 5A). We also examined other
457 nutrient signaling pathways. For example, *aak-1;aak-2* animals lacking the nutrient sensor AMP
458 kinase (AMPK) displayed normal *str-44* expression levels (Figure 5A). Thus, *str-44* expression
459 is not responsive to biogenic amines, internal fat stores, or AMPK signaling.

460 We next tested components of the TOR pathway, another crucial nutrient sensor and regulator of
461 metabolic processes. Loss of the essential TORC1 complex component *raga-1*/RagA modestly
462 reduced fasted *str-44* expression (Figure 5B). In contrast to the inhibitory pathways engaged by
463 the presence of food and food odor, *raga-1* appears to be involved in a positively acting pathway
464 engaged by the absence of food. In addition, loss of the essential TORC2 component *rict-*
465 *1*/Rictor led to a robust increase in *str-44* expression in fed and fasted animals (Figure 5B) and a
466 corresponding behavioral phenotype, increasing butyl acetate attraction (Figure 5D). *rict-1* is
467 broadly expressed, but several of its metabolic functions require expression in the intestine
468 (Soukas et al., 2009). Indeed, we found that the elevated *str-44* expression in *rict-1* mutants was
469 fully rescued by expression of a *rict-1* cDNA in the intestine (Figure 5B). Thus, TORC2
470 signaling in the intestine is a key repressor of *str-44* expression in AWA. Consequently, *rict-1*
471 may be part of a pathway that detects internal nutritional state information and modulates AWA
472 chemoreceptor expression.

473 To identify additional components of the TORC2 signaling pathway that regulates *str-44*, we
474 performed a feeding RNAi screen against known members of the TORC2 pathway (*akt-1*, *let-*
475 *363*, *pkc-2*, *sgk-1*, *sinh-1*, and *skn-1*). Of these, *sgk-1(RNAi)* and *pkc-2(RNAi)* produced an
476 elevation of *str-44* expression similar to *rict-1(RNAi)* (Figure 5C). The TORC2 complex is
477 known to phosphorylate and activate *sgk-1* and *pkc-2* (Jones et al., 2009), suggesting that *rict-1*
478 likely acts through these effectors to suppress *str-44* expression in AWA. We also examined
479 whether loss of any of these genes could suppress the elevated *str-44* expression in *rict-1*
480 mutants, and found that *skn-1(RNAi)* reduced *str-44* expression in this background (Figure 5C).
481 This observation is consistent with previous findings showing that *skn-1* encodes a transcription
482 factor, homologous to Nrf1/2, that is inhibited by *rict-1* signaling (Ruf et al., 2013). Together,

483 these experiments reveal that the nutrient sensing TORC2 pathway functions in the intestine to
484 regulate olfactory receptor expression in AWA.

485 **The pathways that converge upon AWA control olfactory receptor expression and**
486 **behavior in a modular manner**

487 The experiments above identify molecular and neural pathways that allow external and internal
488 cues to influence olfactory receptor expression in AWA. To understand how AWA integrates
489 these signals, we next examined how they interact. We first investigated the pathways that were
490 implicated in crosstalk from food sensory neurons to AWA. Given that the food sensory neurons
491 that inhibit *str-44* expression release insulin peptides, and that the insulin pathway in AWA also
492 influences *str-44* expression, we tested whether the sensory neurons signal to AWA via DAF-
493 2/DAF-16 signaling. Indeed, the elevated expression of *str-44* in *tax-4* sensory-defective mutants
494 or in animals with the ASI sensory neuron silenced was suppressed by the loss of the *daf-*
495 *16*/FOXO transcription factor, a key target of the insulin pathway and other signaling pathways
496 (Figure 6A). This suggests that elevated *str-44* expression due to inactivation of food sensory
497 neurons requires downstream *daf-16*/FOXO signaling. We also found that the enhanced
498 expression of *str-44* caused by hyperactive *goa-1* signaling in AWA was fully suppressed by a
499 *daf-16* mutation (Figure 6A). In addition, silencing of AWA, which reduces *str-44* expression in
500 wild-type animals, had no effect in a *daf-2*/InR mutant (Figure 6—figure supplement 1).
501 Together, these experiments indicate that food sensory neurons signal to AWA via DAF-2-DAF-
502 16 insulin signaling. Changes in AWA activity and G protein signaling that modulate *str-44*
503 expression also depend on the DAF-2-DAF-16 pathway.

504 We next examined whether osmotic stress, which decreases *str-44* expression, operates through
505 any of the pathways identified. Thus, we examined whether osmotic stress during fasting could
506 suppress the elevated *str-44* expression seen in mutant animals lacking *tax-4*, *daf-2*, or *rict-1*.
507 Osmotic stress still had an effect in all of these backgrounds (Figure 6B), suggesting that osmotic
508 stress inhibits *str-44* expression through an as yet unidentified pathway that does not require *tax-*
509 *4, daf-2,* or *rict-1*.

510 Next, we examined how the intestinal *rict-1*/Rictor pathway interacts with the sensory neuron-
511 insulin signaling pathway. A double mutant lacking both *rict-1*/Rictor and *daf-2*/InR showed
512 significantly greater levels of *str-44* expression than each of the single mutants (Figure 6C),
513 suggesting that these two pathways function in parallel to inhibit *str-44* expression. Interestingly,
514 we found that a *rict-1;daf-16* double mutant displayed a phenotype matching *daf-16* single
515 mutants (Figure 6C). This suggests that modulation of *str-44* expression by the intestinal TORC2
516 pathway requires downstream *daf-16*/FOXO signaling in AWA. Given that *rict-1* and *daf-2* act
517 in parallel (the *rict-1;daf-2* double mutant phenotype is more severe than that of the single
518 mutants), *rict-1* likely modulates *daf-16* function through a non-insulin pathway. Together, these
519 results identify several parallel pathways that converge on AWA to control *str-44* expression.
520 These pathways appear to act in a modular manner where they can each independently influence
521 chemoreceptor expression (illustrated in Figure 6D). Regulation of *str-44* by several of these
522 stimuli depends on *daf-16*/FOXO, suggesting that it might serve as a molecular locus of
523 integration.

524 **DISCUSSION**

525

526 Animals respond to sensory cues by generating behavioral responses that reflect their ongoing
527 needs and states. Yet how sensorimotor circuits integrate diverse cues relevant to these needs and
528 modulate their function accordingly is poorly understood. We find that a single *C. elegans*
529 olfactory neuron integrates multiple states and stimuli to influence its expression of olfactory
530 receptors, which in turn alters the animal's food-seeking behaviors. Several molecular and neural
531 pathways that originate in different cell types throughout the body converge on AWA to regulate
532 olfactory receptor expression: crosstalk from other sensory neurons, metabolic signals from the
533 gut, and pathways that signal physiological stress. Our behavioral findings show that the
534 synthesis of these signals by AWA allows animals to generate sensorimotor responses that
535 reflect the animal's overall state. These results suggest a general model in which sensory- and
536 state-dependent transcriptional changes at the sensory periphery modulate animals' sensorimotor
537 responses to meet their ongoing needs and states.

538 We found that AWA olfactory receptor expression reflects recent sensory stimuli, metabolic
539 state, and physiological stress. Recent sensory stimuli are detected by a set of food sensory
540 neurons – ASI, ASK, AWB, BAG, or AQR/PQR/URX – that inhibit AWA olfactory receptor
541 expression in the presence of food. Our data suggest that one possible route of signaling involves
542 the food sensory neurons synapsing onto a second-order neuron in the circuit, AIA, which in turn
543 synapses onto AWA. In addition, sensory neurons may release insulin-like peptides that can
544 activate the DAF-2 insulin receptor in AWA. Given that our experiments suggest a surprisingly
545 high level of crosstalk among the sensory neurons, one possibility is that AWA chemoreceptor
546 expression may reflect the integration of activity across the full chemosensory circuit.
547
548 AWA also integrates metabolic signals from the gut. The TORC2 complex that responds to
549 nutrient levels in the intestine (O'Donnell et al., 2018; Soukas et al., 2009) appears to regulate an
550 as yet unidentified gut-to-brain signaling pathway that impacts AWA olfactory receptor
551 expression. The TORC2 pathway has been shown to impact *daf-28*/insulin-like peptide
552 expression (O'Donnell et al., 2018). However, the *rict-1* mutation enhances *str-44* expression in
553 the *daf-2*/InR mutant, suggesting that *rict-1* also operates through an unidentified pathway that is
554 independent of the insulin pathway.
555
556 Our data are most consistent with a framework in which diverse signaling pathways converge on
557 AWA chemoreceptor expression to allow animals to generate sensorimotor behaviors that may
558 vary across environmental conditions. The modulation of chemoreceptor expression in AWA is
559 unlikely to be explained by a simple homeostatic mechanism in which the purpose of altering
560 chemoreceptors would be to keep AWA activity at a target set point. If this mechanism were in
561 effect, then direct inhibition of AWA activity would be expected to increase the expression of
562 excitatory chemoreceptors; however, we found the opposite to be the case (Figure 4E). Sensory
563 habituation alone is unlikely to be an explanation for the data as exposure to *str-44* odorants does
564 not modify *str-44* expression (Figure 4—figure supplement 2B). In addition, our results cannot
565 be explained by a model where *str-44* expression simply tracks AWA activity, as we find that the
566 high expression level of *str-44* in fasted *daf-2* mutants was not reduced by inhibiting AWA
567 activity (Figure 6—figure supplement 1).
568

569 Although this study focuses largely on two state-dependent chemoreceptors that are expressed in
570 one sensory neuron, our results suggest that >100 olfactory receptors undergo similar state-
571 dependent regulation across multiple classes of sensory neurons (Figure 1). In addition, previous
572 work has shown that the GPCRs *odr-10* and *srh-234* undergo feeding state-dependent regulation
573 (Gruner et al., 2014; Wexler et al., 2020). As *C. elegans* have a relatively small number of
574 olfactory neurons, receptors are an attractive site for sensory flexibility. Consistent with this
575 notion, chemoreceptor genes are frequent targets of evolution that drive naturally occurring
576 changes in behavior (Baldwin et al., 2014; Greene et al., 2016; Nei et al., 2008). Multiple
577 odorants typically activate a single olfactory receptor. Thus, changing the expression of only a
578 few genes could alter responses to many odors. In their natural environment, *C. elegans* are
579 found in soil, compost, or ripe/rotting fruits (Frézal and Félix, 2015). Interestingly, the odors that
580 we identified as ligands for STR-44, propyl and butyl acetate, are major components of the
581 aroma of ripe fruits (López et al., 1998). We also found that *str-44* and *srd-28* drive AWA
582 responses to bacterial odor mixtures. Fruit odors and bacterial odors can both suggest the
583 presence of nearby food to *C. elegans*. The broad tuning of STR-44 to these food and food-
584 adjacent stimuli may allow fasted animals to maximize their chances of encountering food. We
585 expect that other chemoreceptors will be modulated in a similar fashion to control sensory
586 neuron responses and stimulus-specific foraging behaviors.

587 In addition, we found that a large number of non-chemoreceptor neuronal genes are differentially
588 expressed in response to fasting (Supplementary File 1). This result complements previous
589 findings that changes in gene expression are widespread following fasting and in mutants lacking
590 fasting-responsive transcription factors (Harvald et al., 2017; Kaletsky et al., 2016). It is likely
591 that other genes in our dataset contribute to feeding state-dependent changes in neuronal activity
592 and behavior.

593 Our results suggest a potential mechanism by which animals can generate behaviors that reflect
594 an integration of multiple ongoing needs and states. Individual states, like hunger or mating
595 drive, are represented by devoted cell populations that impact many aspects of behavior. For
596 animals to generate behaviors that reflect their overall state, signals from diverse sources need to
597 be integrated by the sensorimotor circuits that implement motivated behaviors. We find that
598 convergent signaling onto neurons in sensorimotor circuits modulates gene expression and thus
599 alters circuit function over long timescales. The inputs onto AWA that convey state information
600 arise from a variety of cell types throughout the body but converge on the *daf-16*/FOXO
601 transcription factor in AWA that controls gene expression. We found that these parallel pathways
602 act in a modular fashion where they can each independently influence chemoreceptor expression,
603 which likely allows animals to adaptively tune their expression of chemoreceptors depending on
604 the sensory cues, stressors, and nutrients in the environment. It is likely that many other neurons
605 in the sensorimotor circuits of *C. elegans* and other animals similarly integrate a wide range of
606 state-relevant inputs to modify their gene expression programs and functional properties.

607 # METHODS AND MATERIALS

608

609 ## KEY RESOURCES TABLE

Reagent type (species) or resource	Designation	Source or reference	Identifiers	Additional information
Strain, strain background (*Caenorhabditis elegans*)	Wild-type Bristol N2	N/A	N2	
Genetic reagent (*Caenorhabditis elegans*)	*odr-7(ky4)*	Sengupta et al, 1996	CX4	
Genetic reagent (*Caenorhabditis elegans*)	*odr-7(ky4); tax-4(p678)*	This study	SWF482	Strain available from Flavell Lab (see Data Availability)
Genetic reagent (*Caenorhabditis elegans*)	*kyIs665[rimb-1::rpl-22-3xHA,myo-3::mCherry]*	This study	CX16283	Strain available from Flavell Lab (see Data Availability)
Genetic reagent (*Caenorhabditis elegans*)	*kyIs587[gpa-6::GCaMP2.2b, unc-122::dsRed]*	Larsch et al, 2013	NZ1101	
Genetic reagent (*Caenorhabditis elegans*)	*srd-28(syb2320)*	This study	PHX2320	Strain available from Flavell Lab (see Data Availability)
Genetic reagent (*Caenorhabditis elegans*)	*str-44(syb1869)*	This study	PHX1869	Strain available from Flavell Lab (see Data Availability)
Genetic reagent (*Caenorhabditis elegans*)	*odr-10(syb3508)*	This study	PHX3508	Strain available from Flavell Lab (see Data Availability)
Genetic reagent (*Caenorhabditis elegans*)	*ser-7(syb1941)*	This study	PHX1941	Strain available from Flavell Lab (see Data Availability)
Genetic reagent (*Caenorhabditis elegans*)	*str-44(syb1869); cat-1(e1111)*	This study	SWF428	Strain available from Flavell Lab (see Data Availability)
Genetic reagent (*Caenorhabditis elegans*)	*str-44(syb3563)IV; srd-28(syb3336)V*	This study	PHX3677	Strain available from Flavell Lab (see Data Availability)
Genetic reagent (*Caenorhabditis elegans*)	*str-44(syb1869);daf-3(e1376)*	This study	SWF456	Strain available from Flavell Lab (see Data Availability)
Genetic reagent (*Caenorhabditis elegans*)	*str-44(syb1869);pdfr-1(ok3425)*	This study	SWF461	Strain available from Flavell Lab (see Data Availability)

Genetic reagent (*Caenorhabditis elegans*)	*odr-7(ky4); tax-4(p678); flvEx283[sra-6::srd-28 cDNA, myo2::mCherry]*	This study	SWF631	Strain available from Flavell Lab (see Data Availability)
Genetic reagent (*Caenorhabditis elegans*)	*odr-7(ky4); tax-4(p678); flvEx181[sra-6::str-44 cDNA, myo-3::mCherry]*	This study	SWF478	Strain available from Flavell Lab (see Data Availability)
Genetic reagent (*Caenorhabditis elegans*)	*tax-4(p678); str-44(syb1869)*	This study	SWF486	Strain available from Flavell Lab (see Data Availability)
Genetic reagent (*Caenorhabditis elegans*)	*str-44(syb1869); ceh-36(ks86)*	This study	SWF514	Strain available from Flavell Lab (see Data Availability)
Genetic reagent (*Caenorhabditis elegans*)	*daf-7(e1372); str-44(syb1869)*	This study	SWF522	Strain available from Flavell Lab (see Data Availability)
Genetic reagent (*Caenorhabditis elegans*)	*daf-2(m41); str-44(syb1869)*	This study	SWF527	Strain available from Flavell Lab (see Data Availability)
Genetic reagent (*Caenorhabditis elegans*)	*str-44(syb1869); flvEx216[Pgpa-6::HisCl]*	This study	SWF528	Strain available from Flavell Lab (see Data Availability)
Genetic reagent (*Caenorhabditis elegans*)	*str-44(syb1869); flvEx239[srh-11::HisCl1-sl2-mCherry(25ng/uL)]*	This study	SWF557	Strain available from Flavell Lab (see Data Availability)
Genetic reagent (*Caenorhabditis elegans*)	*str-44(syb1869); raga-1(ok386)*	This study	SWF545	Strain available from Flavell Lab (see Data Availability)
Genetic reagent (*Caenorhabditis elegans*)	*str-44(syb1869); rict-1(ft7)*	This study	SWF546	Strain available from Flavell Lab (see Data Availability)
Genetic reagent (*Caenorhabditis elegans*)	*str-44(syb1869); flvEx231[srg-47p::HisCl1-sl2-mCherry + myo-3p::mCherry]*	This study	SWF548	Strain available from Flavell Lab (see Data Availability)
Genetic reagent (*Caenorhabditis elegans*)	*str-44(syb1869); flvEx238[tax-4::tax-4 (40ng/uL) + myo-2::mCherry (1ng/uL)]*	This study	SWF552	Strain available from Flavell Lab (see Data Availability)
Genetic reagent (*Caenorhabditis elegans*)	*str-44(syb1869); flvEx239[srh-11::HisCl1-sl2-mCherry(25ng/uL)]*	This study	SWF557	Strain available from Flavell Lab (see Data Availability)
Genetic reagent (*Caenorhabditis elegans*)	*str-44(syb1869); flvEx235 [gcy-33::HisCl1-sl2-mCherry (7.5ng/uL)]*	This study	SWF556	Strain available from Flavell Lab (see Data Availability)

Genetic reagent (*Caenorhabditis elegans*)	*str-44(syb1869); flvEx245[gcy-36::HiCl-sl2-mCherry (2 ng/ul)]*	This study	SWF563	Strain available from Flavell Lab (see Data Availability)
Genetic reagent (*Caenorhabditis elegans*)	*str-44(syb1869); flvEx246[str-1::HiCl-sl2-mCherry (25 ng/ul)]*	This study	SWF564	Strain available from Flavell Lab (see Data Availability)
Genetic reagent (*Caenorhabditis elegans*)	*str-44(syb1869); flvEx241[sra-9::HiCl-sl2-mCherry (25 ng/ul)]*	This study	SWF559	Strain available from Flavell Lab (see Data Availability)
Genetic reagent (*Caenorhabditis elegans*)	*daf-2(m41); str-44(syb1869); flvEx258[gpa-6::daf-2-sl2-mCherry (25ng/uL)]*	This study	SWF583	Strain available from Flavell Lab (see Data Availability)
Genetic reagent (*Caenorhabditis elegans*)	*daf-2(m41); str-44(syb1869); flvEx263[gpa-6::daf-2-sl2-mCherry (25ng/uL)]*	This study	SWF588	Strain available from Flavell Lab (see Data Availability)
Genetic reagent (*Caenorhabditis elegans*)	*str-44(syb1869); mxl-3(ok1947)*	This study	SWF589	Strain available from Flavell Lab (see Data Availability)
Genetic reagent (*Caenorhabditis elegans*)	*str-44(syb1869); flvEx272[gpa-6::acy-1(gf) (25ng/uL), myo-2::mCherry (1ng/uL)]*	This study	SWF611	Strain available from Flavell Lab (see Data Availability)
Genetic reagent (*Caenorhabditis elegans*)	*str-44(syb1869); flvEx279[25ng/uL gpa-6::goa-1(GF)-sl2-mCherry]*	This study	SWF622	Strain available from Flavell Lab (see Data Availability)
Genetic reagent (*Caenorhabditis elegans*)	*str-44(syb1869); daf-16(mu86); flvEx278[25ng/uL gpa-6::daf-16a-sl2-mCherry]*	This study	SWF621	Strain available from Flavell Lab (see Data Availability)
Genetic reagent (*Caenorhabditis elegans*)	*str-44(syb1869); daf-16(mu86); flvEx278[25ng/uL dpy-30::daf-16a-sl2-mCherry]*	This study	SWF625	Strain available from Flavell Lab (see Data Availability)
Genetic reagent (*Caenorhabditis elegans*)	*str-44(syb1869); daf-16(mu86)*	This study	SWF627	Strain available from Flavell Lab (see Data Availability)
Genetic reagent (*Caenorhabditis elegans*)	*flvEx284[ges-1::rict-1 + myo-3::mCherry]; str-44(syb1869); rict-1(ft7)*	This study	SWF633	Strain available from Flavell Lab (see Data Availability)
Genetic reagent (*Caenorhabditis elegans*)	*daf-16(mu86); tax-4(p678); str-44(syb1869)*	This study	SWF638	Strain available from Flavell Lab (see Data Availability)
Genetic reagent (*Caenorhabditis elegans*)	*daf-16(mu86); rict-1(ft7); str-44(syb1869);*	This study	SWF642	Strain available from Flavell Lab (see Data Availability)
Genetic reagent (*Caenorhabditis elegans*)	*str-44(syb1869); flvEx292[ceh-36p::TeTx-SL2-mCherry + myo-3p::mCherry]*	This study	SWF648	Strain available from Flavell Lab (see Data Availability)
Genetic reagent (*Caenorhabditis elegans*)	*str-44(syb1869); flvEx293[gpa-6p::egl-30(gf) + myo-3p::mCherry]*	This study	SWF649	Strain available from Flavell Lab (see Data Availability)

Genetic reagent (*Caenorhabditis elegans*)	*daf-16(mu86); str-44(syb1869); flvEx231[srg-47p::HisCl1-sl2-mCherry + myo-3p::mCherry]*	This study	SWF666	Strain available from Flavell Lab (see Data Availability)
Genetic reagent (*Caenorhabditis elegans*)	*str-44(syb1869); daf-2(m41); flvEx216[gpa-6::HisCl1]*	This study	SWF668	Strain available from Flavell Lab (see Data Availability)
Genetic reagent (*Caenorhabditis elegans*)	*str-44(syb1869); tax-4(p678); flvEx216[gpa-6::HisCl1]*	This study	SWF669	Strain available from Flavell Lab (see Data Availability)
Genetic reagent (*Caenorhabditis elegans*)	*str-44(syb1869); rict-1(ft7); flvEx216[gpa-6::HisCl1]*	This study	SWF670	Strain available from Flavell Lab (see Data Availability)
Genetic reagent (*Caenorhabditis elegans*)	*str-44(syb1869); aak-1(tm1944); aak-2(gt33)*	This study	SWF671	Strain available from Flavell Lab (see Data Availability)
Genetic reagent (*Caenorhabditis elegans*)	*str-44(syb1869);daf-16(mu86); flvEx297[gpa-6::goa-1(gf)-sl2-mCherry (25ng/uL)]*	This study	SWF672	Strain available from Flavell Lab (see Data Availability)
Genetic reagent (*Caenorhabditis elegans*)	*str-44(syb1869);daf-7(e1372); flvEx297[gpa-6::goa-1(gf)-sl2-mCherry (25ng/uL)]*	This study	SWF678	Strain available from Flavell Lab (see Data Availability)
Genetic reagent (*Caenorhabditis elegans*)	*str-44(syb1869); rict-1(ft7); daf-7(e1372)*	This study	SWF679	Strain available from Flavell Lab (see Data Availability)
Genetic reagent (*Caenorhabditis elegans*)	*str44(syb1869); atgl-1(gk176565)*	This study	SWF637	Strain available from Flavell Lab (see Data Availability)
Genetic reagent (*Caenorhabditis elegans*)	*str44(syb1869); lim-4(ky403)*	This study	SWF687	Strain available from Flavell Lab (see Data Availability)
Genetic reagent (*Caenorhabditis elegans*)	*str-44(syb1869); rict-1(ft7); daf-2 (m41)*	This study	SWF699	Strain available from Flavell Lab (see Data Availability)
Genetic reagent (*Caenorhabditis elegans*)	*str-44(syb1869); flvEx350[gpa-6::egl-30(gf) (5ng/uL), myo-2::mCherry (1ng/uL)]*	This study	SWF750	Strain available from Flavell Lab (see Data Availability)
Genetic reagent (*Caenorhabditis elegans*)	*str-44(syb1869); rict-1(ft7); daf-16(mu86)*	This study	SWF642	Strain available from Flavell Lab (see Data Availability)
Genetic reagent (*Caenorhabditis elegans*)	*flvEx390[gpa-6::str-44-sl2-mCherry]*	This study	SWF827	Strain available from Flavell Lab (see Data Availability)
Genetic reagent (*Caenorhabditis elegans*)	*flvEx308[ttx-3::TeTx, myo-3::mCherry]*	This study	SWF698	Strain available from Flavell Lab (see Data Availability)
Genetic reagent (*Caenorhabditis elegans*)	*flvEx307[gcy-28d::TeTx, myo-3::mCherry]*	This study	SWF697	Strain available from Flavell Lab (see Data Availability)

Genetic reagent (*Caenorhabditis elegans*)	*flvEx399[gpa-6::TeTx, myo-3::mCherry]*	This study	SWF843	Strain available from Flavell Lab (see Data Availability)
Genetic reagent (*Caenorhabditis elegans*)	*srd-28(syb2320); daf-16(mu86)*	This study	SWF844	Strain available from Flavell Lab (see Data Availability)
Genetic reagent (*Caenorhabditis elegans*)	*srd-28(syb2320); daf-2(m41)*	This study	SWF845	Strain available from Flavell Lab (see Data Availability)
Genetic reagent (*Caenorhabditis elegans*)	*srd-28(syb2320); tax-4(p678)*	This study	SWF846	Strain available from Flavell Lab (see Data Availability)
Chemical compound, drug	Butyl acetate	Sigma-Aldrich	287725	
Chemical compound, drug	Propyl acetate	Sigma-Aldrich	537438	
Chemical compound, drug	Aztreonam	Sigma-Aldrich	PZ0038	
Software, algorithm	MATLAB	MathWorks	R2014a, R2021b	

Growth conditions and handling

Nematode culture was conducted using standard methods. Populations were maintained on NGM agar plates with *E. coli* OP50 bacteria. Wild-type was *C. elegans* Bristol strain N2. For genetic crosses, genotypes were confirmed using PCR. Transgenic animals were generated by injecting DNA clones plus fluorescent co-injection marker into gonads of young adult hermaphrodites. One day old hermaphrodites were used for all assays. All assays were conducted at room temperature (~22°C). Plates for the osmotic stress experiments were normal NGM plus 150mM sorbitol added. In the presence of this mild stressor, animals displayed altered behaviors such as egg-laying, but do not display acute reversal responses and grow at normal rates (Yu et al., 2017; Zhang et al., 2008).

Plasmid construction

For HisCl1-based silencing of neurons, we inserted the following promoters into pSM-HisCl1-sl2-mCherry: *gpa-6* (AWA), *str-1* (AWB), *gcy-33* (BAG), *srg-47* (ASI), *gcy-36* (URX/AQR/PQR), *sra-9* (ASK), *srh-11* (ASJ). For TeTx-based silencing, we inserted the following promoters into pSM-TeTx-sl2-mCherry: *ceh-36*short (AWC), *gcy-28.d* (AIA), *ttx-3* (AIY).

For AWA-specific expression of HisCl1, *acy-1(gf)*, *goa-1(gf)*, *egl-30(gf)*, *srd-28*, *str-44*, *daf-2*, and *daf-16,* we used the *gpa-6* promoter. *goa-1(gf)* and *egl-30(gf)* were synthesized with the Q205L gain-of-function mutations added at the time of synthesis. These cDNAs were subsequently subcloned into pSM. The *acy-1(gf)* clone was described in a previous study (Flavell et al., 2013). *srd-28* and *str-44* were amplified from pooled cDNA and inserted into the pSM vector. For ASH-specific expression of *str-44* and *srd-28*, we used the *sra-6* promoter. The *daf-16* rescue plasmid was generated by PCR amplifying the *daf-16.a* cDNA from pooled cDNA and

634 inserting it into pSM. The *daf-2* rescue plasmid was generated by excising the *daf-2* cDNA from
635 pJH4531 (a kind gift from M. Zhen) and inserting it into pSM.

636 The *tax-4* and *rict-1* rescue plasmids have been previously described (Macosko et al., 2009;
637 O'Donnell et al., 2018).

638 **CRIPSR gene editing**

639 The T2A-mNeonGreen reporter strains were constructed by inserting a T2A-mNeonGreen
640 coding sequence immediately before the stop codons of *str-44, srd-28*, *odr-10*, and *ser-7* via
641 CRISPR/Cas9 gene editing.

642 The *str-44* mutant was created by introducing an indel at the start codon of the *str-44* gene,
643 resulting in deletion of the start codon. The next internal methionine in *str-44* occurs in the
644 second transmembrane domain and there are no upstream sequences that could result in an in-
645 frame start codon, suggesting that this should result in a null mutation. The *srd-28* mutant was
646 created by introducing a frameshift indel near the beginning of the second coding exon of *srd-28*,
647 which is a large exon that encodes three of the seven transmembrane domains.

648 **Translating ribosome affinity purification and analysis**

649 Translating ribosome affinity purification was performed as described as in a previously
650 published detailed protocol (McLachlan and Flavell, 2019). Briefly, a ribotagging plasmid was
651 constructed containing the *C. elegans rpl-22* cDNA with three tandem HA tags under control of
652 the *rimb-1* (previously *tag-168*) pan-neuronal promoter. Animals containing an integrated copy
653 of this transgene were grown on 15cm enriched-peptone (20 g/L) NGM plates seeded throughout
654 with OP50 to one-day old adults, then washed to fresh plates with or without OP50 lawns seeded
655 one day prior. After three hours, animals were collected with liquid NGM supplemented with
656 cycloheximide (0.8 mg/mL) and flash frozen within minutes. Samples were then prepared for
657 lysis and RNA isolation as previously described. We performed three independent biological
658 replicates in total.

659 Whole animal and ribotag RNA samples were amplified with the Clontech SMART-Seq v2 Low
660 Input RNA kit and prepared as Illumina Nextera XT libraries by the MIT BioMicroCenter
661 sequencing core. Reads were mapped to the *C. elegans* genome (WBcel235) with kallisto (Bray
662 et al., 2016) and analyzed for differential expression with sleuth (Pimentel et al., 2017) and
663 custom scripts. Data are deposited at GEO accession number GSE200640. For the data shown in
664 Figure 1 and Supplementary File 1, we required that each enriched gene was four-fold enriched
665 in the differential expression analysis.

666 **Confocal imaging and quantification**

667 For experiments using the *str-44*p::mNeonGreen reporter, animals were imaged with the same
668 laser power, exposure time, and objective lens to allow for comparisons between experimental
669 conditions. For each experimental condition, 20-30 animals were immobilized in 5 mM
670 tetramisole hydrochloride (Sigma) on a #1.5 coverslip, then mounted on slides with minimally
671 thick NGM pads. Data were collected on a Nikon Eclipse Ti microscope coupled to a Yokogawa
672 CSU-X1 spinning disk unit with a Borealis upgrade. We used a 40x/1.15NA CFI Apo LWD

673 Lambda water immersion objective and NIS Elements software for data acquisition. Z-stacks
674 were collected through the entire depth of the animal at 0.5 micron steps. Fluorescence intensity
675 was quantified in ImageJ (NIH). For each animal, a maximum intensity z-projection containing
676 the neuron nearest the objective was generated, a box was drawn around the neuron, and an
677 intensity profile was generated from the box. A single background-subtracted fluorescence
678 intensity value was calculated for each cell by subtracting the mean bottom 5% of fluorescent
679 signal (background) from the mean top 5% of fluorescent signal (neural signal). To aid
680 comparisons between experiments, these values were normalized to the mean of fed wild-type
681 control animals imaged on the same day. Violin plots were generated with a custom MATLAB
682 function (Bastian Bechtold, Violin Plots for Matlab, https://github.com/bastibe/Violinplot-
683 Matlab).

684 **Food choice assay**

685 The binary food choice assay was performed as previous described (Worthy et al., 2018) with
686 minor modifications. OP50 bacteria were grown overnight with agitation in LB media at 37°C,
687 centrifuged at 5000 rpm for 2 minutes, and resuspended in fresh LB to OD600 = 10. 6 cm NGM
688 plates were spotted with two drops of 25 µL each, air dried for 10 minutes, then covered with a
689 lid and incubated at room temperature (22°C) for 5 hours. 2 µL of odorant or ethanol vehicle was
690 added adjacent to the bacterial lawns immediately prior to adding animals to the plate. Adult
691 animals were washed twice in S. Basal buffer and 40-200 animals were placed near the center of
692 the plate, equidistant from the bacterial patches, and the plate was covered with a lid. Following
693 standard protocols (Worthy et al., 2018), animals were immobilized by adding 5 µL of 1M
694 sodium azide to each bacterial patch after 1 hour. Animals inside each patch were counted, and a
695 food choice index was calculated as animals within experimental patch / animals within both
696 patches.

697 **Exploration assays and recordings of locomotion**

698 Behavioral assays for on-food exploration were conducted as previously described (Flavell et al.,
699 2013) with minor modifications. One-day old adults were washed off growth plates and fed on
700 OP50 lawns (seeded the day before) or fasted off-food for three hours. Individual animals were
701 then picked to 60mm plates uniformly seeded with OP50 and allowed to freely locomote for five
702 hours. After this time, animals were removed from the lawn, and plates were superimposed on a
703 grid containing 3.5mm squares and the number of squares containing worm tracks were
704 manually counted.

705 For quantification of animal speed in the absence of food, one-day old adult animals were
706 washed from OP50 plates with liquid NGM and, after three washes, were transferred to 10cm
707 NGM plates with copper filter paper (Whatman paper soaked in 0.02 M $CuCl_2$) boundaries.
708 Animals were recorded for 1hr on JAI Spark SP-20000M cameras with Streampix 7 software at
709 3 fps, and speed was extracted from videos using custom Matlab scripts as previously described
710 (Rhoades et al, 2019).

711 **Culture and use of diverse bacterial species**

712 For experiments involving species other than *E. coli* OP50, all bacterial species (PA14, DA1877,
713 JUB19, MYB71, BigB0393) were streaked onto LB plates from frozen stocks and plates were
714 incubated overnight at 25°C. A sterile pipette tip was used to pick colonies from the plate into
715 LB medium for an overnight incubation at 37°C. NGM plates were seeded with 200µL of the
716 bacteria respectively for the feeding experiments followed by confocal imaging as described
717 above. JUB19, MYB71, and BigB0393 are courtesy of the CeMbio collection at the
718 *Caenorhabditis* Genetics Center.

719 For food on lid (odor) experiments done on PA14 and DA1877, bacteria were cultured as
720 described above. A thin NGM pad was placed on the lid with 150 µL of OD600 = 1 bacteria.
721 This was chosen due to previous work on PA14 inducing aversive olfactory learning that used
722 this same concentration (Zhang et al, 2005).

723 **Feeding with aztreonam-treated bacteria**

724 To aztreonam-treat bacteria, a standard OP50 culture was diluted 5-fold in LB with 5 µg/mL
725 aztreonam and grown overnight at 37°C with gentle agitation. Bacteria were then plated on
726 NGM plates with 10 µg/mL aztreonam. Bacteria were allowed to grow overnight at room
727 temperature, then visually inspected for filamentous growth before animals were plated for the
728 experiment.

729 **RNA interference screen**

730 Animals were fed on bacteria containing RNAi feeding vectors from the Ahringer (Kamath et al.,
731 2003) (for *unc-22, akt-1, skn-1, rict-1,* and *let-363)* or ORFeome (Rual et al., 2004) (for *sinh*-1,
732 *sgk-1*, and *pkc-2*) libraries. Bacteria were plated in a uniform lawn on 6 cm NGM plates with the
733 addition of 25 µg/mL carbenicillin and 1 mM IPTG. To avoid maternal effect, embryonic
734 lethality, and early developmental defects from RNAi, as well as starvation associated with
735 standard L1 synchronization, *str-44*::T2A-mNeonGreen animals were allowed to lay eggs on
736 standard NGM plates seeded with OP50, then the hatched progeny were washed with M9 onto
737 feeding RNAi plates at L1-L2 stage. Animals were imaged as young adults (~2 days later) only
738 when *unc-22* positive control plates produced twitching animals.

739 **Chemotaxis assays**

740 Chemotaxis assays were performed as previously described (Bargmann 1993). Assays were
741 conducted on square grid plates of assay agar, poured the night before the assay. Assays were
742 conducted in a 22°C incubator set to 40% humidity. One day old adult animals were washed off
743 growth plates using S Basal buffer, then washed twice more with S. Basal and once with water.
744 50-200 animals were placed on the chemotaxis plates. Two 1 µL spots of odor were placed on
745 one side of the plate, and two 1 µL spots of ethanol on the opposite side (ethanol was used as the
746 dilutant for all odors). Two 1 µL spots of 1 M sodium azide were placed on either end of the
747 plate to paralyze animals at the odor source. Animals navigated the plate for 60 minutes (except
748 90 minutes for the *tax-4; odr-7* worms and those in that background, as their locomotion was
749 slower). Plates were then placed in a 4°C cold room to arrest movement. The assay was scored
750 by counting animals that arrived at the odor, at the control ethanol spot, or elsewhere in the plate.

751 This was used to calculate a Chemotaxis Index, ($\#_{odor}$ - $\#_{ethanol}$)/ ($\#_{odor}$ + $\#_{ethanol}$ + $\#_{other}$). Worms in
752 the center of the assay plate that did not move from their starting position were excluded.

753 Odor concentrations used were as follows: 1:1000 diacetyl, 1:1000 methyl pyrazine, 10 mg/mL
754 pyrazine, 1:10 butyl acetate, 1:10 propyl acetate, 1:100 hexyl acetate, 1:100 ethyl acetate, 1:100
755 isoamyl acetate.

756 **Calcium imaging in freely-moving animals**

757 In vivo calcium imaging of AWA::GCaMP2.2b in freely-moving animals was carried out on a
758 Nikon Eclipse Ti-S microscope with a 2x/0.10NA Plan Apo objective and an Andor Zyla 4.2
759 Plus sCMOS camera. Blue light application to animals from an X-Cite 120LED system was
760 10ms for each exposure, at a frame rate of 10 fps. For these experiments, slides were prepared by
761 placing a 2 µL drop of OP50 (OD600 = 2) on a minimally thick NGM pad, then a custom cut
762 PDMS corral was placed on the pad. Five animals were picked (without food) to the center of the
763 corral (off food) and covered with a coverslip, then immediately imaged. Animals began outside
764 the field of view of the objective lens and were allowed to freely navigate into the bacterial lawn
765 within the field of view. Individual slides were imaged for no longer than 30 minutes.
766 Background-subtracted intensity values for AWA were extracted from each video frame using
767 custom ImageJ macros, as described previously (Flavell et al., 2013). Food patch encounter
768 frames were manually annotated. $\Delta F/F_0$ was calculated as (fluorescence – baseline)/baseline,
769 where fluorescence is a 10 frame (one second) moving median and baseline is the 5th percentile
770 fluorescence throughout the recording.

771 **Calcium imaging during odor delivery in immobilized animals**

772 Imaging of neurons was performed as previously described (Chute et al., 2019).
773 AWA::GCaMP2.2b animals were picked as larval stage 4 (L4) hermaphrodites the day prior to
774 imaging, and singled onto a NGM plate seeded with OP50. The animals were kept at 20°C for 16
775 hours. The next day they were imaged as young adults. Animals were loaded into a modified
776 PDMS olfactory chip(Reilly et al., 2017) only allowing the animal's nose to be subjected to the
777 solution. Well-fed worms were transferred directly from the NGM plate into the chip. Fasted
778 animals were transferred to an unseeded NGM plate 3 hours prior to imaging and then
779 transferred into the chip. Animals were imaged under 40x magnification for two 30 second trials.
780 Each trial consisted of a 5 sec period prior to stimulation, a 10sec odor pulse, and a 15 sec
781 recording post stimulation. The recording was performed in Micro-Manager recording TIFF
782 stacks at 10 frames/ second, exciting the neuron with blue light at 470 nm. A minimum of 10
783 animals (or 20 trials) was captured for each condition.

784 The solutions used for imaging were all made in S. Basal (100.103 mM NaCl, 5.741 mM
785 K_2HPO_4, 44.090 mM KH_2PO_4, 0.0129 mM Cholesterol in H_2O). The solvent control solution was
786 1 mM tetramisole, 0.3 µM fluorescein in S. Basal. The flow control solution, not exposed to the
787 worm but controlling the movement of the solutions in the olfactory chip, was 1mM tetramisole,
788 0.6µM fluorescein in S. Basal. The stimuli were 10^{-6} propyl acetate or butyl acetate, prepared by
789 serial dilutions in solvent control solution.

Images were analyzed using ImageJ software. For AWA imaging, the fluorescence change in the soma was measured and selected as the region of interest. The fluorescence of an equally sized region of interest was captured from the background. The fluorescence of the background was then subtracted from the neuron for each frame to obtain background-subtracted fluorescence. F/F_0 was then calculated by dividing each frame by F_0 (average fluorescence from seconds 2-3 of each trial). This adjusted F/F_0 value was corrected to be the percent change in fluorescence by the following equation: $(F/F_0 - 1) * 100\%$.

The maximum change in fluorescence was calculated for each trial. The maximum value for the "Pre" is defined as the maximum percent change in fluorescence from 0.0-4.9 seconds. The "Stim" period was 5.0-15.0 seconds. The "Post" period was 15.1-29.9 seconds.

MATERIALS AND DATA AVAILABILITY

All materials (strains and reagents) generated for this study are freely available upon request, and all data are publicly available. RNA sequencing data is deposited at GEO accession number GSE200640. Other data (fluorescent reporter and calcium imaging data) is deposited on Dryad at doi:10.5061/dryad.t4b8gtj4h.

ACKNOWLEDGMENTS

We thank Donovan Ventimiglia, Paul Greer, Matthew Lovett-Barron, Eviatar Yemini, Taralyn Tan, and members of the Flavell lab for critical reading of the manuscript. We thank Mei Zhen, Michael O'Donnell, and Piali Sengupta for plasmids, and the Caenorhabditis Genetics Center (supported by P40 OD010440), Horvitz lab, and Bargmann lab for strains. We thank the MIT BioMicroCenter for RNA library preparation and sequencing. I.G.M. was supported by the Picower Fellows program. J.S. acknowledges funding from NIH (DC016058). S.W.F. acknowledges funding from the JPB Foundation, NIH (NS104892), NSF (#1845663), McKnight Foundation, and Alfred P. Sloan Foundation.

DECLARATIONS OF INTERESTS

The authors declare that they have no competing interests.

REFERENCES

Aponte, Y., Atasoy, D., Sternson, S.M., 2011. AGRP neurons are sufficient to orchestrate feeding behavior rapidly and without training. Nat. Neurosci. 14, 351–355. https://doi.org/10.1038/nn.2739

Avery, L., Horvitz, H.R., 1990. Effects of starvation and neuroactive drugs on feeding in Caenorhabditis elegans. J. Exp. Zool. 253, 263–270. https://doi.org/10.1002/jez.1402530305

Baldwin, M.W., Toda, Y., Nakagita, T., O'Connell, M.J., Klasing, K.C., Misaka, T., Edwards, S.V., Liberles, S.D., 2014. Sensory biology. Evolution of sweet taste perception in hummingbirds by transformation of the ancestral umami receptor. Science 345, 929–933. https://doi.org/10.1126/science.1255097

830 Ben Arous, J., Laffont, S., Chatenay, D., 2009. Molecular and sensory basis of a food related
831 two-state behavior in C. elegans. PloS One 4, e7584.
832 https://doi.org/10.1371/journal.pone.0007584
833 Bentley, B., Branicky, R., Barnes, C.L., Chew, Y.L., Yemini, E., Bullmore, E.T., Vértes, P.E.,
834 Schafer, W.R., 2016. The Multilayer Connectome of Caenorhabditis elegans. PLoS
835 Comput. Biol. 12, e1005283. https://doi.org/10.1371/journal.pcbi.1005283
836 Bray, N.L., Pimentel, H., Melsted, P., Pachter, L., 2016. Near-optimal probabilistic RNA-seq
837 quantification. Nat. Biotechnol. 34, 525–527. https://doi.org/10.1038/nbt.3519
838 Chalasani, S.H., Chronis, N., Tsunozaki, M., Gray, J.M., Ramot, D., Goodman, M.B., Bargmann,
839 C.I., 2007. Dissecting a circuit for olfactory behaviour in Caenorhabditis elegans. Nature
840 450, 63–70. https://doi.org/10.1038/nature06292
841 Chen, C., Itakura, E., Nelson, G.M., Sheng, M., Laurent, P., Fenk, L.A., Butcher, R.A., Hegde,
842 R.S., de Bono, M., 2017. IL-17 is a neuromodulator of Caenorhabditis elegans sensory
843 responses. Nature 542, 43–48. https://doi.org/10.1038/nature20818
844 Chew, Y.L., Tanizawa, Y., Cho, Y., Zhao, B., Yu, A.J., Ardiel, E.L., Rabinowitch, I., Bai, J.,
845 Rankin, C.H., Lu, H., Beets, I., Schafer, W.R., 2018. An Afferent Neuropeptide System
846 Transmits Mechanosensory Signals Triggering Sensitization and Arousal in C. elegans.
847 Neuron 99, 1233-1246.e6. https://doi.org/10.1016/j.neuron.2018.08.003
848 Chute, C.D., DiLoreto, E.M., Zhang, Y.K., Reilly, D.K., Rayes, D., Coyle, V.L., Choi, H.J.,
849 Alkema, M.J., Schroeder, F.C., Srinivasan, J., 2019. Co-option of neurotransmitter
850 signaling for inter-organismal communication in C. elegans. Nat. Commun. 10, 3186.
851 https://doi.org/10.1038/s41467-019-11240-7
852 Clark, J.T., Kalra, P.S., Crowley, W.R., Kalra, S.P., 1984. Neuropeptide Y and human
853 pancreatic polypeptide stimulate feeding behavior in rats. Endocrinology 115, 427–429.
854 https://doi.org/10.1210/endo-115-1-427
855 De Rosa, M.J., Veuthey, T., Florman, J., Grant, J., Blanco, M.G., Andersen, N., Donnelly, J.,
856 Rayes, D., Alkema, M.J., 2019. The flight response impairs cytoprotective mechanisms
857 by activating the insulin pathway. Nature 573, 135–138. https://doi.org/10.1038/s41586-
858 019-1524-5
859 Ferkey, D.M., Sengupta, P., L'Etoile, N.D., 2021. Chemosensory signal transduction in
860 Caenorhabditis elegans. Genetics 217, iyab004.
861 https://doi.org/10.1093/genetics/iyab004
862 Flavell, S.W., Gogolla, N., Lovett-Barron, M., Zelikowsky, M., 2022. The emergence and
863 influence of internal states. Neuron S0896-6273(22)00407-X.
864 https://doi.org/10.1016/j.neuron.2022.04.030
865 Flavell, S.W., Gordus, A., 2022. Dynamic functional connectivity in the static connectome of
866 Caenorhabditis elegans. Curr. Opin. Neurobiol. 73, 102515.
867 https://doi.org/10.1016/j.conb.2021.12.002
868 Flavell, S.W., Pokala, N., Macosko, E.Z., Albrecht, D.R., Larsch, J., Bargmann, C.I., 2013.
869 Serotonin and the neuropeptide PDF initiate and extend opposing behavioral states in C.
870 elegans. Cell 154, 1023–1035. https://doi.org/10.1016/j.cell.2013.08.001
871 Flavell, S.W., Raizen, D.M., You, Y.-J., 2020. Behavioral States. Genetics 216, 315–332.
872 https://doi.org/10.1534/genetics.120.303539
873 Frézal, L., Félix, M.-A., 2015. C. elegans outside the Petri dish. eLife 4.
874 https://doi.org/10.7554/eLife.05849
875 Ghosh, D.D., Sanders, T., Hong, S., McCurdy, L.Y., Chase, D.L., Cohen, N., Koelle, M.R.,
876 Nitabach, M.N., 2016. Neural Architecture of Hunger-Dependent Multisensory Decision
877 Making in C. elegans. Neuron 92, 1049–1062.
878 https://doi.org/10.1016/j.neuron.2016.10.030

879 Greene, J.S., Dobosiewicz, M., Butcher, R.A., McGrath, P.T., Bargmann, C.I., 2016. Regulatory
880 changes in two chemoreceptor genes contribute to a Caenorhabditis elegans QTL for
881 foraging behavior. eLife 5, e21454. https://doi.org/10.7554/eLife.21454
882 Gruner, M., Nelson, D., Winbush, A., Hintz, R., Ryu, L., Chung, S.H., Kim, K., Gabel, C.V., van
883 der Linden, A.M., 2014. Feeding state, insulin and NPR-1 modulate chemoreceptor gene
884 expression via integration of sensory and circuit inputs. PLoS Genet. 10, e1004707.
885 https://doi.org/10.1371/journal.pgen.1004707
886 Harvald, E.B., Sprenger, R.R., Dall, K.B., Ejsing, C.S., Nielsen, R., Mandrup, S., Murillo, A.B.,
887 Larance, M., Gartner, A., Lamond, A.I., Færgeman, N.J., 2017. Multi-omics Analyses of
888 Starvation Responses Reveal a Central Role for Lipoprotein Metabolism in Acute
889 Starvation Survival in C. elegans. Cell Syst. 5, 38-52.e4.
890 https://doi.org/10.1016/j.cels.2017.06.004
891 Hawk, J.D., Calvo, A.C., Liu, P., Almoril-Porras, A., Aljobeh, A., Torruella-Suárez, M.L., Ren, I.,
892 Cook, N., Greenwood, J., Luo, L., Wang, Z.-W., Samuel, A.D.T., Colón-Ramos, D.A.,
893 2018. Integration of Plasticity Mechanisms within a Single Sensory Neuron of C. elegans
894 Actuates a Memory. Neuron 97, 356-367.e4.
895 https://doi.org/10.1016/j.neuron.2017.12.027
896 Hilbert, Z.A., Kim, D.H., 2017. Sexually dimorphic control of gene expression in sensory
897 neurons regulates decision-making behavior in C. elegans. eLife 6, e21166.
898 https://doi.org/10.7554/eLife.21166
899 Hill, A.J., Mansfield, R., Lopez, J.M.N.G., Raizen, D.M., Van Buskirk, C., 2014. Cellular stress
900 induces a protective sleep-like state in C. elegans. Curr. Biol. CB 24, 2399–2405.
901 https://doi.org/10.1016/j.cub.2014.08.040
902 Hindmarsh Sten, T., Li, R., Otopalik, A., Ruta, V., 2021. Sexual arousal gates visual processing
903 during Drosophila courtship. Nature 595, 549–553. https://doi.org/10.1038/s41586-021-
904 03714-w
905 Hoopfer, E.D., Jung, Y., Inagaki, H.K., Rubin, G.M., Anderson, D.J., 2015. P1 interneurons
906 promote a persistent internal state that enhances inter-male aggression in Drosophila.
907 eLife 4, e11346. https://doi.org/10.7554/eLife.11346
908 Horio, N., Liberles, S.D., 2021. Hunger enhances food-odour attraction through a neuropeptide
909 Y spotlight. Nature 592, 262–266. https://doi.org/10.1038/s41586-021-03299-4
910 Iliff, A.J., Xu, X.Z.S., 2020. C. elegans: a sensible model for sensory biology. J. Neurogenet. 34,
911 347–350. https://doi.org/10.1080/01677063.2020.1823386
912 Inagaki, H.K., Panse, K.M., Anderson, D.J., 2014. Independent, reciprocal neuromodulatory
913 control of sweet and bitter taste sensitivity during starvation in Drosophila. Neuron 84,
914 806–820. https://doi.org/10.1016/j.neuron.2014.09.032
915 Ji, N., Madan, G.K., Fabre, G.I., Dayan, A., Baker, C.M., Kramer, T.S., Nwabudike, I., Flavell,
916 S.W., 2021. A neural circuit for flexible control of persistent behavioral states. eLife 10,
917 e62889. https://doi.org/10.7554/eLife.62889
918 Johnson, A.K., Gross, P.M., 1993. Sensory circumventricular organs and brain homeostatic
919 pathways. FASEB J. Off. Publ. Fed. Am. Soc. Exp. Biol. 7, 678–686.
920 https://doi.org/10.1096/fasebj.7.8.8500693
921 Jones, K.T., Greer, E.R., Pearce, D., Ashrafi, K., 2009. Rictor/TORC2 regulates Caenorhabditis
922 elegans fat storage, body size, and development through sgk-1. PLoS Biol. 7, e60.
923 https://doi.org/10.1371/journal.pbio.1000060
924 Jourjine, N., Mullaney, B.C., Mann, K., Scott, K., 2016. Coupled Sensing of Hunger and Thirst
925 Signals Balances Sugar and Water Consumption. Cell 166, 855–866.
926 https://doi.org/10.1016/j.cell.2016.06.046
927 Kaletsky, R., Lakhina, V., Arey, R., Williams, A., Landis, J., Ashraf, J., Murphy, C.T., 2016. The
928 C. elegans adult neuronal IIS/FOXO transcriptome reveals adult phenotype regulators.
929 Nature 529, 92–96. https://doi.org/10.1038/nature16483

930 Kim, D.H., Flavell, S.W., 2020. Host-microbe interactions and the behavior of Caenorhabditis
931 elegans. J. Neurogenet. 34, 500–509. https://doi.org/10.1080/01677063.2020.1802724
932 Ko, K.I., Root, C.M., Lindsay, S.A., Zaninovich, O.A., Shepherd, A.K., Wasserman, S.A., Kim,
933 S.M., Wang, J.W., 2015. Starvation promotes concerted modulation of appetitive
934 olfactory behavior via parallel neuromodulatory circuits. eLife 4.
935 https://doi.org/10.7554/eLife.08298
936 Krashes, M.J., Koda, S., Ye, C., Rogan, S.C., Adams, A.C., Cusher, D.S., Maratos-Flier, E.,
937 Roth, B.L., Lowell, B.B., 2011. Rapid, reversible activation of AgRP neurons drives
938 feeding behavior in mice. J. Clin. Invest. 121, 1424–1428.
939 https://doi.org/10.1172/JCI46229
940 Kruk, M.R., Van der Poel, A.M., Meelis, W., Hermans, J., Mostert, P.G., Mos, J., Lohman, A.H.,
941 1983. Discriminant analysis of the localization of aggression-inducing electrode
942 placements in the hypothalamus of male rats. Brain Res. 260, 61–79.
943 https://doi.org/10.1016/0006-8993(83)90764-3
944 Landis, J.N., Murphy, C.T., 2010. Integration of diverse inputs in the regulation of
945 Caenorhabditis elegans DAF-16/FOXO. Dev. Dyn. Off. Publ. Am. Assoc. Anat. 239,
946 1405–1412. https://doi.org/10.1002/dvdy.22244
947 Larsch, J., Ventimiglia, D., Bargmann, C.I., Albrecht, D.R., 2013. High-throughput imaging of
948 neuronal activity in Caenorhabditis elegans. Proc. Natl. Acad. Sci. U. S. A. 110, E4266-
949 4273. https://doi.org/10.1073/pnas.1318325110
950 Lin, D., Boyle, M.P., Dollar, P., Lee, H., Lein, E.S., Perona, P., Anderson, D.J., 2011. Functional
951 identification of an aggression locus in the mouse hypothalamus. Nature 470, 221–226.
952 https://doi.org/10.1038/nature09736
953 López, M.L., Lavilla, M.T., Riba, M., Vendrell, M., 1998. Comparison of Volatile Compounds in
954 Two Seasons in Apples: Golden Delicious and Granny Smith. J. Food Qual. 21, 155–
955 166.
956 Luquet, S., Perez, F.A., Hnasko, T.S., Palmiter, R.D., 2005. NPY/AgRP neurons are essential
957 for feeding in adult mice but can be ablated in neonates. Science 310, 683–685.
958 https://doi.org/10.1126/science.1115524
959 Macosko, E.Z., Pokala, N., Feinberg, E.H., Chalasani, S.H., Butcher, R.A., Clardy, J.,
960 Bargmann, C.I., 2009. A hub-and-spoke circuit drives pheromone attraction and social
961 behaviour in C. elegans. Nature 458, 1171–1175. https://doi.org/10.1038/nature07886
962 McLachlan, I.G., Flavell, S.W., 2019. Cell Type-specific mRNA Purification in Caenorhabditis
963 elegans via Translating Ribosome Affinity Purification. Bio-Protoc. 9, e3328.
964 https://doi.org/10.21769/BioProtoc.3328
965 Meisel, J.D., Panda, O., Mahanti, P., Schroeder, F.C., Kim, D.H., 2014. Chemosensation of
966 bacterial secondary metabolites modulates neuroendocrine signaling and behavior of C.
967 elegans. Cell 159, 267–280. https://doi.org/10.1016/j.cell.2014.09.011
968 Murphy, C.T., Hu, P.J., 2013. Insulin/insulin-like growth factor signaling in C. elegans.
969 WormBook Online Rev. C Elegans Biol. 1–43. https://doi.org/10.1895/wormbook.1.164.1
970 Nath, R.D., Chow, E.S., Wang, H., Schwarz, E.M., Sternberg, P.W., 2016. C. elegans Stress-
971 Induced Sleep Emerges from the Collective Action of Multiple Neuropeptides. Curr. Biol.
972 CB 26, 2446–2455. https://doi.org/10.1016/j.cub.2016.07.048
973 Nei, M., Niimura, Y., Nozawa, M., 2008. The evolution of animal chemosensory receptor gene
974 repertoires: roles of chance and necessity. Nat. Rev. Genet. 9, 951–963.
975 https://doi.org/10.1038/nrg2480
976 Nelson, M.D., Lee, K.H., Churgin, M.A., Hill, A.J., Van Buskirk, C., Fang-Yen, C., Raizen, D.M.,
977 2014. FMRFamide-like FLP-13 neuropeptides promote quiescence following heat stress
978 in Caenorhabditis elegans. Curr. Biol. CB 24, 2406–2410.
979 https://doi.org/10.1016/j.cub.2014.08.037

980 O'Donnell, M.P., Chao, P.-H., Kammenga, J.E., Sengupta, P., 2018. Rictor/TORC2 mediates
981 gut-to-brain signaling in the regulation of phenotypic plasticity in C. elegans. PLoS
982 Genet. 14, e1007213. https://doi.org/10.1371/journal.pgen.1007213
983 Ohno, H., Sakai, N., Adachi, T., Iino, Y., 2017. Dynamics of Presynaptic Diacylglycerol in a
984 Sensory Neuron Encode Differences between Past and Current Stimulus Intensity. Cell
985 Rep. 20, 2294–2303. https://doi.org/10.1016/j.celrep.2017.08.038
986 Oka, Y., Ye, M., Zuker, C.S., 2015. Thirst driving and suppressing signals encoded by distinct
987 neural populations in the brain. Nature 520, 349–352.
988 https://doi.org/10.1038/nature14108
989 Pimentel, H., Bray, N.L., Puente, S., Melsted, P., Pachter, L., 2017. Differential analysis of RNA-
990 seq incorporating quantification uncertainty. Nat. Methods 14, 687–690.
991 https://doi.org/10.1038/nmeth.4324
992 Pokala, N., Liu, Q., Gordus, A., Bargmann, C.I., 2014. Inducible and titratable silencing of
993 Caenorhabditis elegans neurons in vivo with histamine-gated chloride channels. Proc.
994 Natl. Acad. Sci. U. S. A. 111, 2770–2775. https://doi.org/10.1073/pnas.1400615111
995 Reilly, D.K., Lawler, D.E., Albrecht, D.R., Srinivasan, J., 2017. Using an Adapted Microfluidic
996 Olfactory Chip for the Imaging of Neuronal Activity in Response to Pheromones in Male
997 C. Elegans Head Neurons. J. Vis. Exp. JoVE. https://doi.org/10.3791/56026
998 Rhoades, J.L., Nelson, J.C., Nwabudike, I., Yu, S.K., McLachlan, I.G., Madan, G.K., Abebe, E.,
999 Powers, J.R., Colón-Ramos, D.A., Flavell, S.W., 2019. ASICs Mediate Food Responses
1000 in an Enteric Serotonergic Neuron that Controls Foraging Behaviors. Cell 176, 85-
1001 97.e14. https://doi.org/10.1016/j.cell.2018.11.023
1002 Root, C.M., Ko, K.I., Jafari, A., Wang, J.W., 2011. Presynaptic facilitation by neuropeptide
1003 signaling mediates odor-driven food search. Cell 145, 133–144.
1004 https://doi.org/10.1016/j.cell.2011.02.008
1005 Ruf, V., Holzem, C., Peyman, T., Walz, G., Blackwell, T.K., Neumann-Haefelin, E., 2013.
1006 TORC2 signaling antagonizes SKN-1 to induce C. elegans mesendodermal embryonic
1007 development. Dev. Biol. 384, 214–227. https://doi.org/10.1016/j.ydbio.2013.08.011
1008 Ryan, D.A., Miller, R.M., Lee, K., Neal, S.J., Fagan, K.A., Sengupta, P., Portman, D.S., 2014.
1009 Sex, age, and hunger regulate behavioral prioritization through dynamic modulation of
1010 chemoreceptor expression. Curr. Biol. CB 24, 2509–2517.
1011 https://doi.org/10.1016/j.cub.2014.09.032
1012 Samuel, B.S., Rowedder, H., Braendle, C., Félix, M.-A., Ruvkun, G., 2016. Caenorhabditis
1013 elegans responses to bacteria from its natural habitats. Proc. Natl. Acad. Sci. U. S. A.
1014 113, E3941-3949. https://doi.org/10.1073/pnas.1607183113
1015 Sawin, E.R., Ranganathan, R., Horvitz, H.R., 2000. C. elegans locomotory rate is modulated by
1016 the environment through a dopaminergic pathway and by experience through a
1017 serotonergic pathway. Neuron 26, 619–631. https://doi.org/10.1016/s0896-
1018 6273(00)81199-x
1019 Sayin, S., De Backer, J.-F., Siju, K.P., Wosniack, M.E., Lewis, L.P., Frisch, L.-M., Gansen, B.,
1020 Schlegel, P., Edmondson-Stait, A., Sharifi, N., Fisher, C.B., Calle-Schuler, S.A.,
1021 Lauritzen, J.S., Bock, D.D., Costa, M., Jefferis, G.S.X.E., Gjorgjieva, J., Grunwald
1022 Kadow, I.C., 2019. A Neural Circuit Arbitrates between Persistence and Withdrawal in
1023 Hungry Drosophila. Neuron 104, 544-558.e6.
1024 https://doi.org/10.1016/j.neuron.2019.07.028
1025 Shtonda, B.B., Avery, L., 2006. Dietary choice behavior in Caenorhabditis elegans. J. Exp. Biol.
1026 209, 89–102. https://doi.org/10.1242/jeb.01955
1027 Skora, S., Mende, F., Zimmer, M., 2018. Energy Scarcity Promotes a Brain-wide Sleep State
1028 Modulated by Insulin Signaling in C. elegans. Cell Rep. 22, 953–966.
1029 https://doi.org/10.1016/j.celrep.2017.12.091

Soukas, A.A., Kane, E.A., Carr, C.E., Melo, J.A., Ruvkun, G., 2009. Rictor/TORC2 regulates fat metabolism, feeding, growth, and life span in Caenorhabditis elegans. Genes Dev. 23, 496–511. https://doi.org/10.1101/gad.1775409

Srinivasan, S., Sadegh, L., Elle, I.C., Christensen, A.G.L., Faergeman, N.J., Ashrafi, K., 2008. Serotonin regulates C. elegans fat and feeding through independent molecular mechanisms. Cell Metab. 7, 533–544. https://doi.org/10.1016/j.cmet.2008.04.012

Suzuki, H., Thiele, T.R., Faumont, S., Ezcurra, M., Lockery, S.R., Schafer, W.R., 2008. Functional asymmetry in Caenorhabditis elegans taste neurons and its computational role in chemotaxis. Nature 454, 114–117. https://doi.org/10.1038/nature06927

Takeishi, A., Yeon, J., Harris, N., Yang, W., Sengupta, P., 2020. Feeding state functionally reconfigures a sensory circuit to drive thermosensory behavioral plasticity. eLife 9, e61167. https://doi.org/10.7554/eLife.61167

Taylor, S.R., Santpere, G., Weinreb, A., Barrett, A., Reilly, M.B., Xu, C., Varol, E., Oikonomou, P., Glenwinkel, L., McWhirter, R., Poff, A., Basavaraju, M., Rafi, I., Yemini, E., Cook, S.J., Abrams, A., Vidal, B., Cros, C., Tavazoie, S., Sestan, N., Hammarlund, M., Hobert, O., Miller, D.M., 2021. Molecular topography of an entire nervous system. Cell 184, 4329-4347.e23. https://doi.org/10.1016/j.cell.2021.06.023

Wexler, L.R., Miller, R.M., Portman, D.S., 2020. C. elegans Males Integrate Food Signals and Biological Sex to Modulate State-Dependent Chemosensation and Behavioral Prioritization. Curr. Biol. CB 30, 2695-2706.e4. https://doi.org/10.1016/j.cub.2020.05.006

White, J.G., Southgate, E., Thomson, J.N., Brenner, S., 1986. The structure of the nervous system of the nematode Caenorhabditis elegans. Philos. Trans. R. Soc. Lond. B. Biol. Sci. 314, 1–340. https://doi.org/10.1098/rstb.1986.0056

Witham, E., Comunian, C., Ratanpal, H., Skora, S., Zimmer, M., Srinivasan, S., 2016. C. elegans Body Cavity Neurons Are Homeostatic Sensors that Integrate Fluctuations in Oxygen Availability and Internal Nutrient Reserves. Cell Rep. 14, 1641–1654. https://doi.org/10.1016/j.celrep.2016.01.052

Witvliet, D., Mulcahy, B., Mitchell, J.K., Meirovitch, Y., Berger, D.R., Wu, Y., Liu, Y., Koh, W.X., Parvathala, R., Holmyard, D., Schalek, R.L., Shavit, N., Chisholm, A.D., Lichtman, J.W., Samuel, A.D.T., Zhen, M., 2021. Connectomes across development reveal principles of brain maturation. Nature 596, 257–261. https://doi.org/10.1038/s41586-021-03778-8

Worthy, S.E., Haynes, L., Chambers, M., Bethune, D., Kan, E., Chung, K., Ota, R., Taylor, C.J., Glater, E.E., 2018. Identification of attractive odorants released by preferred bacterial food found in the natural habitats of C. elegans. PloS One 13, e0201158. https://doi.org/10.1371/journal.pone.0201158

Yapici, N., Cohn, R., Schusterreiter, C., Ruta, V., Vosshall, L.B., 2016. A Taste Circuit that Regulates Ingestion by Integrating Food and Hunger Signals. Cell 165, 715–729. https://doi.org/10.1016/j.cell.2016.02.061

Yu, J., Yang, W., Liu, H., Hao, Y., Zhang, Y., 2017. An Aversive Response to Osmotic Upshift in Caenorhabditis elegans. eNeuro 4, ENEURO.0282-16.2017. https://doi.org/10.1523/ENEURO.0282-16.2017

Zaslaver, A., Liani, I., Shtangel, O., Ginzburg, S., Yee, L., Sternberg, P.W., 2015. Hierarchical sparse coding in the sensory system of Caenorhabditis elegans. Proc. Natl. Acad. Sci. U. S. A. 112, 1185–1189. https://doi.org/10.1073/pnas.1423656112

Zhang, M., Chung, S.H., Fang-Yen, C., Craig, C., Kerr, R.A., Suzuki, H., Samuel, A.D.T., Mazur, E., Schafer, W.R., 2008. A self-regulating feed-forward circuit controlling C. elegans egg-laying behavior. Curr. Biol. CB 18, 1445–1455. https://doi.org/10.1016/j.cub.2008.08.047

Zhang, Y., Lu, H., Bargmann, C.I., 2005. Pathogenic bacteria induce aversive olfactory learning in Caenorhabditis elegans. Nature 438, 179–184. https://doi.org/10.1038/nature04216

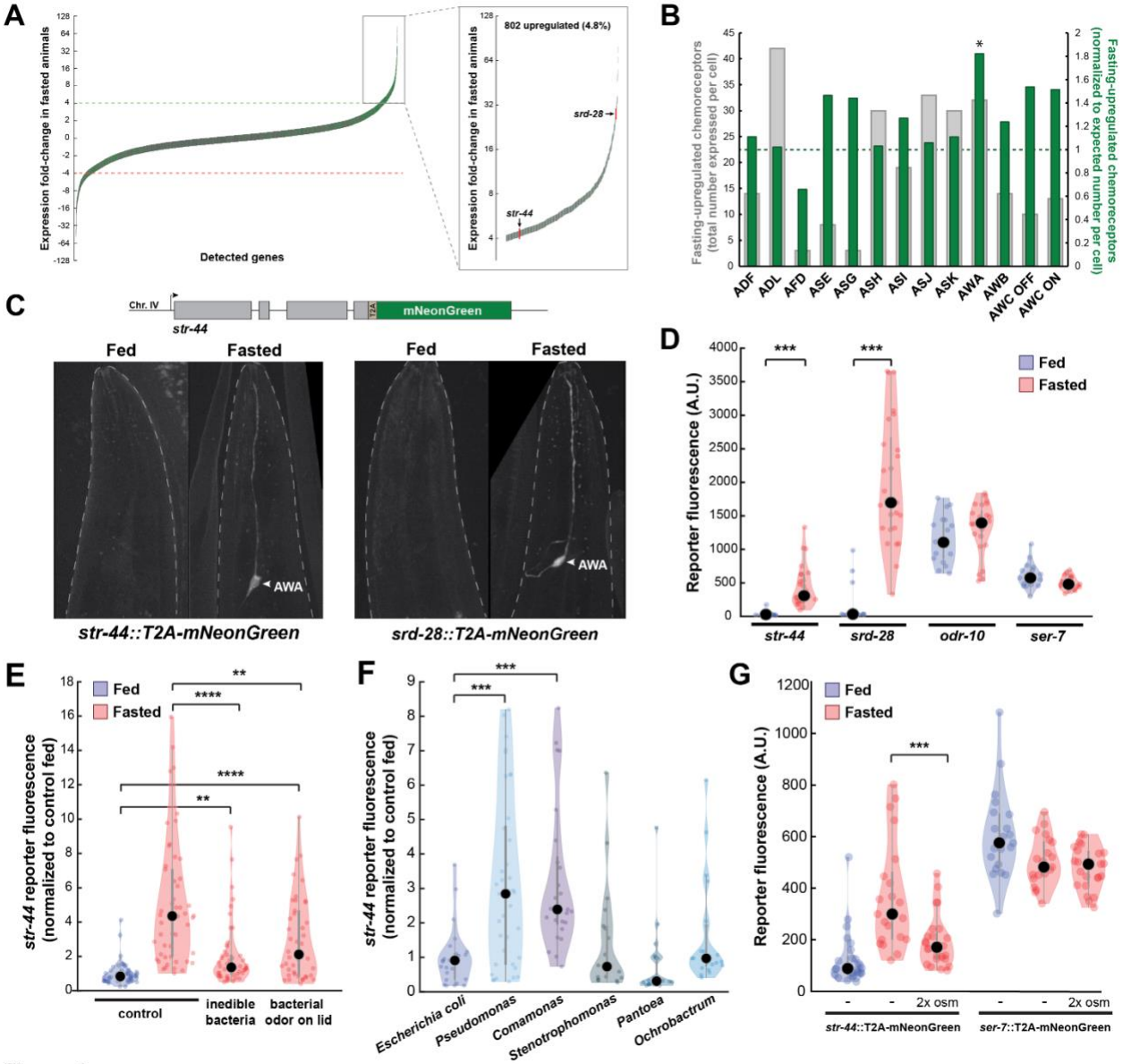

1081 **Figure 1**

1082 **Figure 1. Diverse states and stimuli influence the expression of chemosensory GPCRs in the**
1083 **AWA olfactory neuron**
1084 (A) Fold-change of transcript levels for all detected genes (n = 16,591) after three hours of
1085 fasting compared to well-fed condition. Dashed lines represent the fold-change cutoff for
1086 upregulated (green) or downregulated (red) genes. Green: chemoreceptors; gray: all other genes.
1087 Inset: zoomed view of upregulated genes.
1088 (B) Number of upregulated chemoreceptors in each of the 12 amphid neurons, based on the
1089 CeNGEN expression database. Gray bars: total number of upregulated chemoreceptor genes
1090 expressed per neuron. Dark green bars: fraction of upregulated chemoreceptors per neuron,
1091 divided by the fraction of all chemoreceptors expressed in that neuron (i.e. enrichment of fasting-
1092 upregulated chemoreceptors in each neuron, compared to number expected by chance based on
1093 total number of chemoreceptors in the neuron). *$p < 0.05$, Bonferroni-corrected Chi-Squared
1094 Test.
1095 (C) Top: Endogenous CRISPR/Cas9 tagging strategy to visualize chemoreceptor gene expression
1096 *in vivo*, in which a T2A-mNeonGreen reporter sequence was inserted immediately before the
1097 stop codon. Bottom: Example images of reporter strains in fed and fasted states. AWA neuron is
1098 indicated by arrowhead.
1099 (D) Quantification of chemoreceptor reporter gene fluorescence for two state-dependent
1100 chemoreceptors (*str-44* and *srd-28*), the known AWA chemoreceptor *odr-10*, and a control
1101 GPCR (*ser-7*) that is not upregulated by fasting. Note that there is no significant difference
1102 between fed and fasted for *odr-10* and *ser-7* reporters.
1103 (E) Relative expression of *str-44*::T2A-mNeonGreen in animals fed or fasted for three hours,
1104 animals exposed to inedible aztreonam-treated bacteria for three hours, and animals fasted in the
1105 presence of odors from an unreachable bacterial lawn (on lid of plate).
1106 (F) Relative expression *of str-44*::T2A-mNeonGreen in animals reared on *E. coli* (OP50) then
1107 fed on different bacteria for three hours. Bacterial strains used: OP50 (*E. coli*), PA14
1108 (*Pseudomonas*), DA1877 (*Comamonas*), JUb19 (*Stenotrophomonas*), BIGb0393 (*Pantoea*),
1109 Myb71 (*Ochrobactrum*).
1110 (G) Expression of *str-44*::T2A-mNeonGreen and *ser*-7::T2A-mNeonGreen (negative control)
1111 fed, fasted for three hours, or fasted on 300 mOsm plates (NGM supplemented with an extra 150
1112 mM sorbitol). Note that there is no significant effect of mild osmotic stress on the *ser-7* reporter.
1113
1114 For (D-G), colored dots represent measurements from individual cells, black dots represent
1115 median values, and shaded area shows kernel density estimation for the data. Each condition
1116 measured in two independent sessions. ***$p < 0.001$, **$p < 0.01$, *$p < 0.05$, two-tailed t-test
1117 with Bonferroni correction.

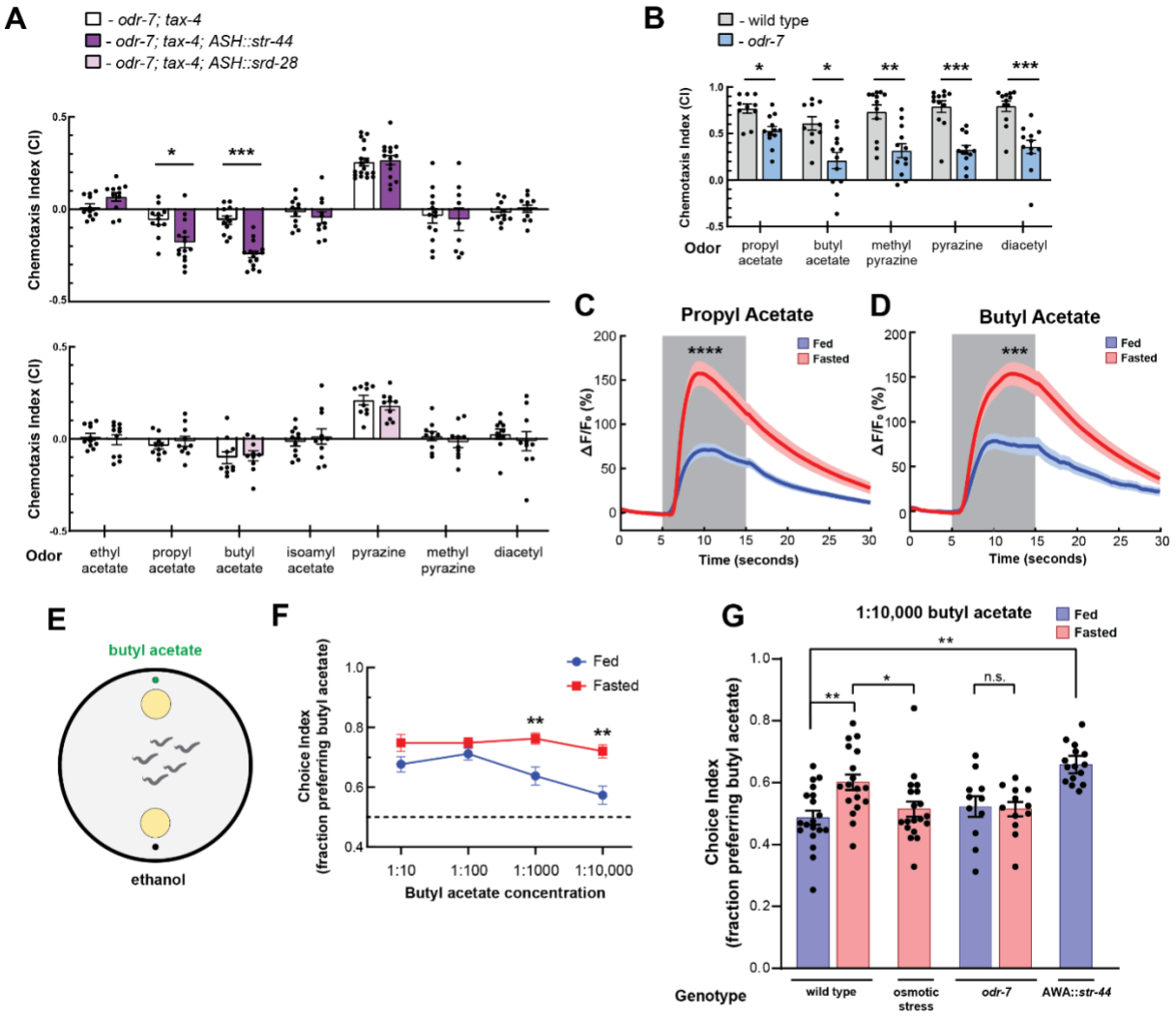

Figure 2

1118

1119 **Figure 2. The state-dependent chemoreceptor *str-44* responds to appetitive odors and**
1120 **controls state-dependent odor preference**
1121 (A) Chemotaxis behavior in *odr-7(ky4);tax-4(p678)* animals, and *odr-7;tax-4* animals expressing
1122 either *str-44* or *srd-28* in the nociceptive neuron ASH (*sra-6p*). Bars show mean ± SEM. n = 2-4
1123 days, each with 3-6 assay plates per odor, and 50-200 animals per plate. (*p < 0.01, ***p <
1124 0.001, t-test with Bonferroni correction)
1125 (B) Chemotaxis behavior to odors of interest in wild type and *odr-7* mutants, which lack a
1126 functional AWA neuron. Bars show mean ± SEM. n = 2 days, each with 5-7 assay plates per
1127 odor. (* p < 0.01, ** p < 0.005, ***p < 0.001, t-test with Bonferroni correction). *odr-7* mutant
1128 chemotaxis to a wide range of other odors is not impaired (Sengupta et al, 1994)
1129 (C) AWA calcium imaging in response to a 10 second addition of 10^{-6} propyl acetate in fed
1130 (blue) and 3 hour fasted (red) worms. n = 31 fed animals, 13 fasted animals, two trials per
1131 animal. Plots show mean ± SEM. ****p < 0.0001, t-test with Bonferroni correction.
1132 (D) AWA calcium imaging in response to 10 second addition of 10^{-6} butyl acetate in fed (blue)
1133 and 3 hour fasted (red) worms. n = 20 fed animals, 14 fasted animals, two trials per animal. Plots
1134 show mean ± SEM. ***p < 0.001, t-test with Bonferroni correction.
1135 (E) Schematic of food choice assay. Animals are placed equidistant from two *E. coli* OP50
1136 lawns, one with an adjacent drop of butyl acetate and one with an adjacent drop of ethanol (its
1137 dilutant).
1138 (F) Food choice behavior of fed and fasted animals, showing fraction of animals that chose the
1139 food lawn with a spot of butyl acetate at the indicated concentration. Plots show mean ± SEM. n
1140 = 9-20 plates per odor over two independent sessions, each with 40-200 animals. **p < 0.01, t-
1141 test with Bonferroni correction.
1142 (G) Food choice behavior of fed and fasted WT or mutant animals, animals experiencing osmotic
1143 stress during fasting, and fed animals overexpressing *str-44* in AWA (*gpa-6p*), showing fraction
1144 of animals that chose the food lawn with a spot of 1:10,000 butyl acetate. Bars show mean ±
1145 SEM. n > 12 plates per odor over two independent sessions, each with 40-200 animals. ****p <
1146 0.0001, **p < 0.01, t-test with Bonferroni correction. Note that there is no significant effect
1147 between fed and fasted for *odr-7* mutants.

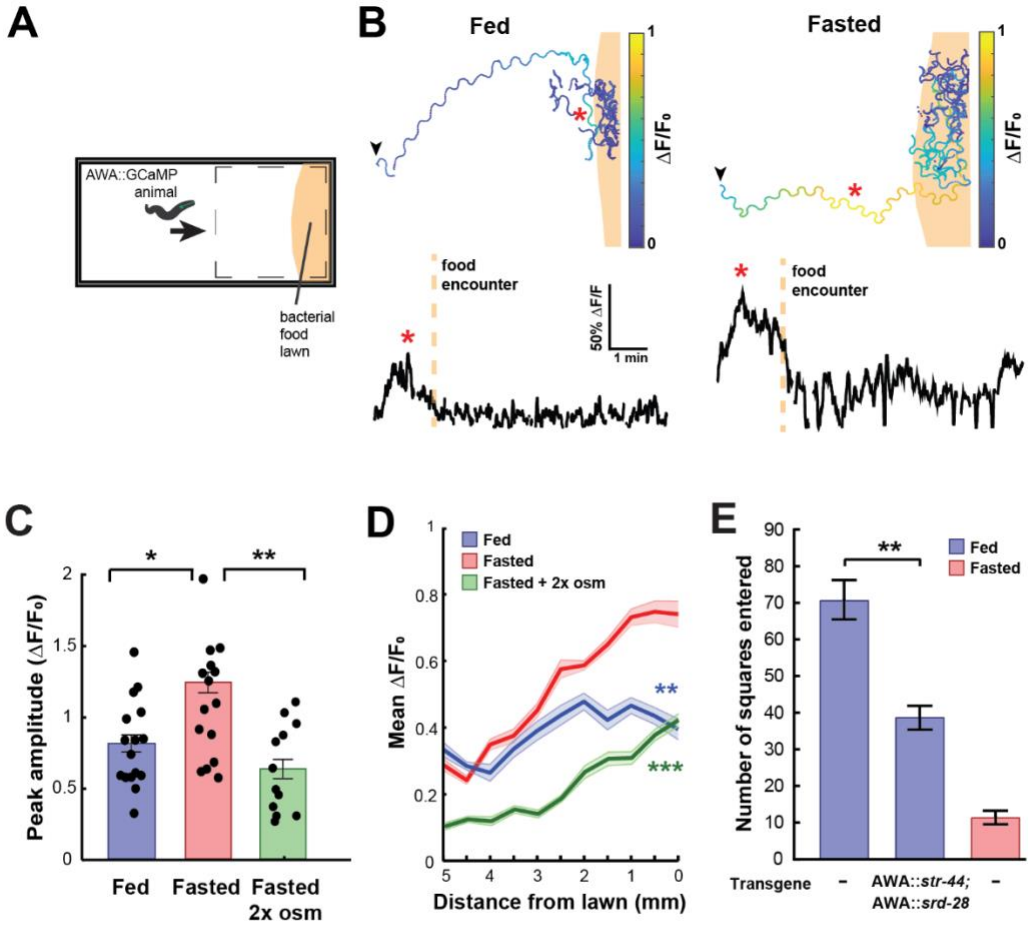
A
AWA::GCaMP
animal
bacterial
food
lawn
B
Fed
Fasted
ΔF/F₀
food
encounter
50% ΔF/F
1 min
C
Peak amplitude (ΔF/F₀)
Fed
Fasted
Fasted
2x osm
D
Fed
Fasted
Fasted + 2x osm
Mean ΔF/F₀
Distance from lawn (mm)
E
Number of squares entered
Fed
Fasted
Transgene
AWA::str-44;
AWA::srd-28

Figure 3

1150 **Figure 3. State-dependent AWA calcium responses and behavioral responses to bacterial**
1151 **food**
1152
1153 (A) Schematic of freely moving calcium imaging assay. Animals expressing AWA::GCaMP2.2b
1154 are picked to an agar pad and allowed to freely navigate to an *E. coli* OP50 lawn. Dashed box
1155 indicates field of view of the microscope.
1156 (B) Example AWA GCaMP recording of an individual fed (left) or fasted (right) animal. Top:
1157 movement trajectories of animals, with colors indicating AWA GCaMP fluorescence. Bottom:
1158 GCaMP trace for the same animals. Red asterisks: peak of GCaMP signal. Dashed line: time of
1159 food encounter.
1160 (C) Amplitude of each GCaMP peak in fed animals, fasted animals, and animals fasted in the
1161 presence of osmotic stress (300 mOsm). Bars show mean ± SEM. *$p < 0.05$, **$p < 0.01$, t-test
1162 with Bonferroni correction.
1163 (D) Mean GCaMP signal in fed or fasted animals binned by the animal's distance from the lawn
1164 boundary (0.5mm bins). n = 18 animals per condition. Plots show mean ± SEM. Two-way
1165 ANOVA, significant effect of feeding state ***$p < 0.001$, **$p < 0.01$).
1166 (E) On-food exploration assay comparing wild-type fed and fasted animals with fed animals
1167 overexpressing *str-44* and *srd-28* chemoreceptors in AWA (*gpa-6p*). n = 15-30 animals per
1168 condition. Plots show mean ± SEM. **$p< 0.01$, t-test.

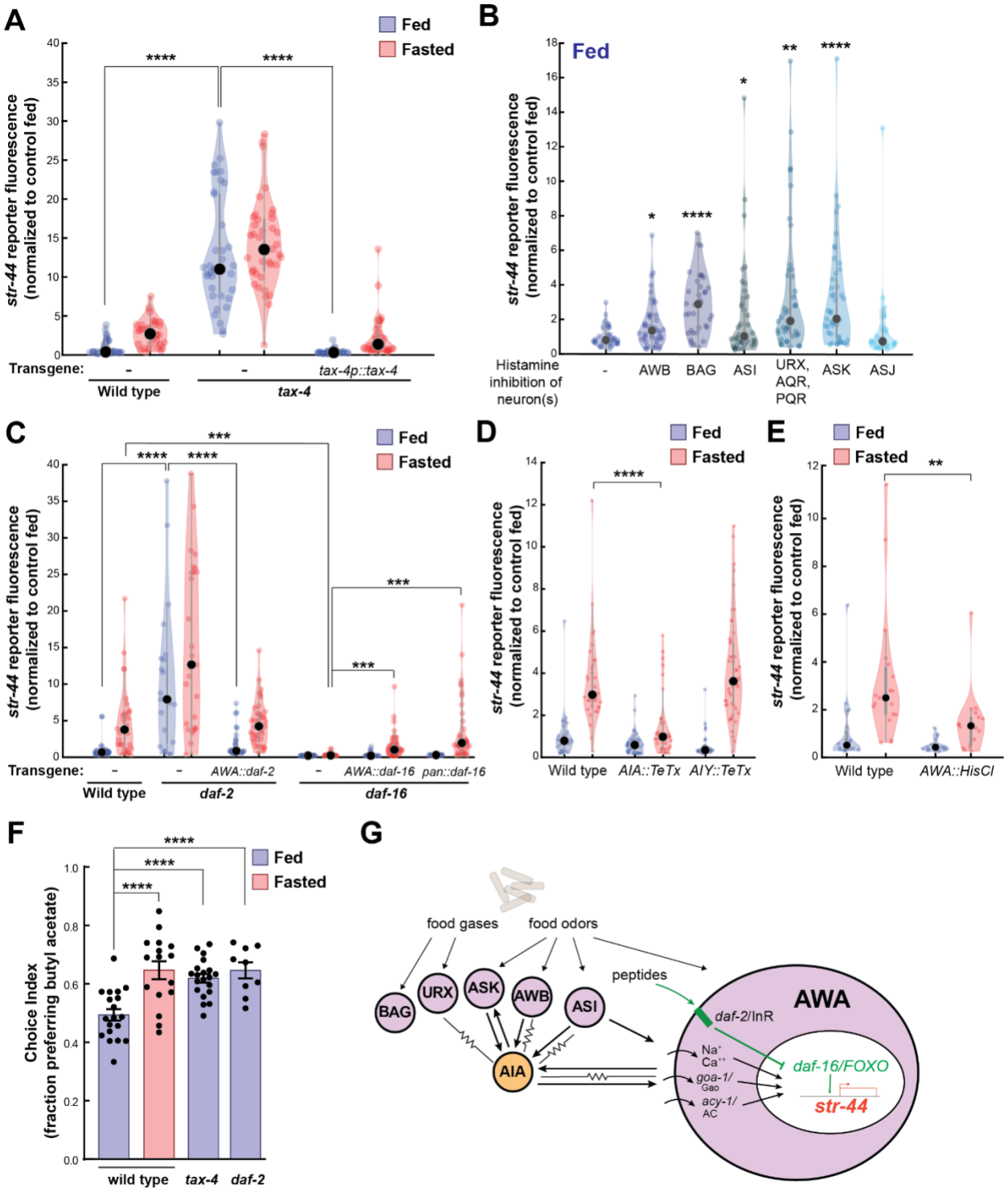
A
Fed
Fasted
str-44 reporter fluorescence (normalized to control fed)
Transgene:
-
-
tax-4p::tax-4
Wild type
tax-4
B
Fed
Histamine inhibition of neuron(s)
-
AWB
BAG
ASI
URX, AQR, PQR
ASK
ASJ
C
Transgene:
-
-
AWA::daf-2
-
AWA::daf-16
pan::daf-16
Wild type
daf-2
daf-16
D
Wild type
AIA::TeTx
AIY::TeTx
E
AWA::HisCl
F
Choice Index (fraction preferring butyl acetate)
wild type
tax-4
daf-2
G
food gases
food odors
peptides
BAG
URX
ASK
AWB
ASI
AIA
AWA
daf-2/InR
daf-16/FOXO
str-44
Na+
Ca++
goa-1/ Gao
acy-1/ AC

Figure 4

1171 **Figure 4. Signaling from food sensory neurons to AWA modulates *str-44* expression via**
1172 **multiple pathways**
1173 (A) Relative expression of *str-44*::T2A-mNeonGreen in *tax-4(p678)* mutants with and
1174 without *tax-4*::*tax-4* rescue construct, compared to wild type. **** $p < 0.0001$, two-tailed t-test
1175 with Bonferroni correction.
1176 (B) *str-44*::T2A-mNeonGreen expression following 3 hour histamine-induced inhibition of
1177 sensory neurons while feeding. Histamine-gated chloride channel (HisCl1) transgenes expressed
1178 with cell-specific promoters: AWB (*str-1*p::HisCl1), BAG (*gcy-33*p::HisCl1), ASI (*srg-*
1179 *47*p::HisCl1), URX, AQR, PQR (*gcy-36*p::HisCl), ASK (*sra-9*p::HisCl1), ASJ (*srh-*
1180 *11*p::HisCl1). *$p < 0.05$, **$p < 0.01$, ***$p < 0.001$, ****$p < 0.0001$, two-tailed t-test with
1181 Bonferroni correction. Note that there is no significant effect of ASJ silencing, compared to
1182 controls.
1183 (C) Relative expression of *str-44*::T2A-mNeonGreen in *daf-2(m41)*, and *daf-16(mu86)* mutants
1184 and mutants bearing transgenes for AWA-specific (*gpa-6*p) or pan-body (*dpy-30*p) rescues
1185 for *daf-2* and *daf-16*. ***$p < 0.001$, ****$p < 0.0001$, two-tailed t-test with Bonferroni correction.
1186 (D) Relative expression of *str-44*::T2A-mNeonGreen in animals with synaptic silencing of AIA
1187 (*gcy-28.d*p::TeTx) or AIY (*ttx-3*p::TeTx). ****$p < 0.0001$, two-tailed t-test with Bonferroni
1188 correction. Note that there is no significant effect of AIY synaptic silencing, compared to
1189 controls.
1190 (E) Relative expression of *str-44*::T2A-mNeonGreen following 3 hour histamine induced
1191 inhibition of AWA (*gpa-6*p::HisCl1). **$p < 0.01$, two-tailed t-test with Bonferroni correction.
1192 (F) Food choice behavior in wild type, *tax-4*, or *daf-2* mutant animals showing fraction of
1193 animals that chose the food lawn with a spot of 1:10,000 butyl acetate. Bars show mean ± SEM.
1194 $n > 15$ plates per odor over two independent sessions, each with 40-200 animals. ****$p <$
1195 0.0001, t-test with Bonferroni correction.
1196 (G) Model depicting the pathways that signal from food sensory neurons to AWA. Signaling
1197 occurs via insulin signaling, modulation of AWA activity, and modulation of AWA G protein
1198 signaling.
1199
1200 For (A-E), colored dots represent measurements from individual cells, black dots represent
1201 median values, shaded area shows kernel density estimation for the data. Each condition
1202 measured in two independent sessions.

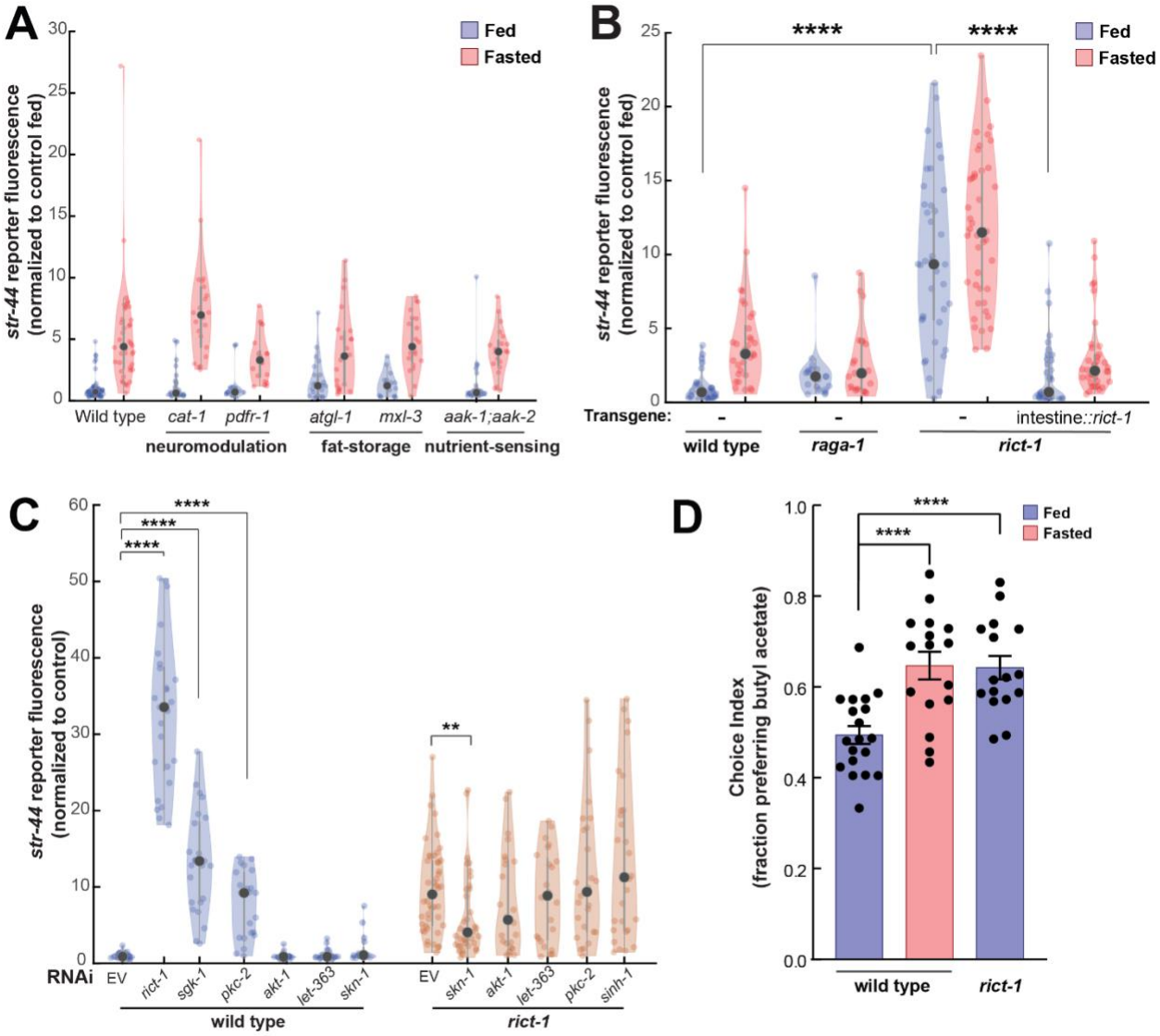
A
Fed
Fasted
str-44 reporter fluorescence (normalized to control fed)
Wild type
cat-1
pdfr-1
atgl-1
mxl-3
aak-1;aak-2
neuromodulation
fat-storage
nutrient-sensing
B
****
****
Fed
Fasted
str-44 reporter fluorescence (normalized to control fed)
Transgene:
intestine::rict-1
wild type
raga-1
rict-1
C
****
****
****
**
str-44 reporter fluorescence (normalized to control)
RNAi
EV
rict-1
sgk-1
pkc-2
akt-1
let-363
skn-1
sinh-1
wild type
rict-1
D
****
****
Fed
Fasted
Choice Index (fraction preferring butyl acetate)
wild type
rict-1

Figure 5

1204 **Figure 5. TORC2 signaling from the gut controls AWA *str-44* expression and odor**
1205 **preference**
1206 (A) Relative expression of *str-44*::T2A-mNeonGreen in *cat-1(e1111)*, *pdfr-1(ok3425)*, *atgl-*
1207 *1(gk176565)*, *mxl-3(ok1947), aak-1(tm1944);aak-2(gt33)* mutants compared to wild-type. All
1208 mutant genotypes shown are statistically indistinguishable from the corresponding wild-type
1209 controls, and all fed versus starved comparisons within each genotype are significant at $p < 0.001$
1210 (two-tailed t-test).
1211 (B) Relative expression of *str-44*::T2A-mNeonGreen in *raga-1(ok386)* and *rict-1(ft7)* mutants
1212 and *rict-1* mutant bearing transgene for intestinal-specific (*ges-1p*) rescue for *rict-1(ft-7)*
1213 compared to wild-type when fed and fasted. *raga-1(ok386)* fed versus starved comparison is not
1214 significant by two-tailed t-test ($p > .05$).
1215 (C) Relative expression of *str-44*::T2A-mNeonGreen in animals fed on *E. coli* HT115 with
1216 empty RNAi vector, *rict-1(RNAi)*, *sgk-1(RNAi)*, *pkc-2(RNAi), akt-1(RNAi), let-363(RNAi), skn-*
1217 *1(RNAi),* or *sinh-1(RNAi)*. Left: wild type animals fed on RNAi. Right: *rict-1(ft7)* mutant
1218 animals fed on RNAi to identify suppressors. Unless otherwise marked, RNAi of genes resulted
1219 in no significant difference from controls.
1220 (D) Food choice behavior in wild type or *rict-1* mutant animals showing fraction of animals that
1221 chose the food lawn with a spot of 1:10,000 butyl acetate. Bars show mean ± SEM. $n > 15$ plates
1222 per odor over two independent sessions, each with 40-200 animals. ****$p < 0.0001$, t-test with
1223 Bonferroni correction.
1224
1225 For (A-C), each condition measured in two independent sessions. ****$p < 0.0001$, **$p < 0.01$by
1226 two-tailed t-test. Colored dots represent from individual cells, black dots represent median
1227 values, shaded area shows kernel density estimation for the data.

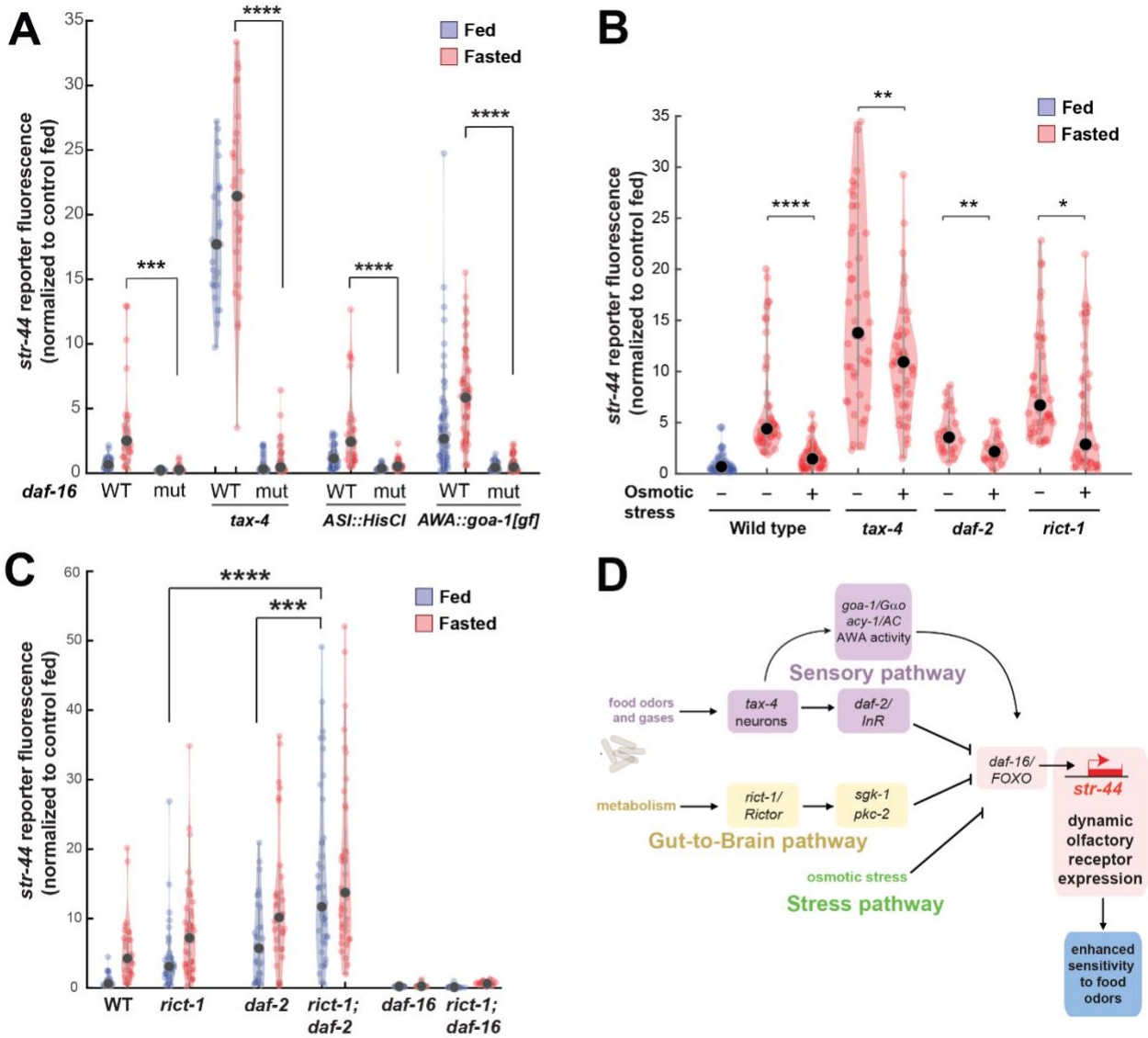
A
str-44 reporter fluorescence (normalized to control fed)
Fed
Fasted
daf-16
WT
mut
tax-4
ASI::HisCl
AWA::goa-1[gf]
B
Osmotic stress
Wild type
tax-4
daf-2
rict-1
C
WT
rict-1
daf-2
rict-1; daf-2
daf-16
rict-1; daf-16
D
goa-1/Gαo
acy-1/AC
AWA activity
Sensory pathway
food odors and gases
tax-4 neurons
daf-2/ InR
daf-16/ FOXO
str-44
dynamic olfactory receptor expression
enhanced sensitivity to food odors
metabolism
rict-1/ Rictor
sgk-1
pkc-2
Gut-to-Brain pathway
osmotic stress
Stress pathway

Figure 6

1229 **Figure 6. Food sensory signals, gut-to-brain metabolic signals, and stress pathways act in a**
1230 **parallel, modular fashion to control *str-44* expression**
1231 (A) Relative expression of *str-44*::T2A-mNeonGreen in wild type, *daf-16, tax-4, tax-4;daf-16,*
1232 *ASI::HisCl. ASI::HisCl;daf-16, AWA::goa-1, AWA::goa-1;daf-16* animals.
1233 (B) Relative expression of *str-44*::T2A-mNeonGreen in wild type, *tax-4*, *daf-2*, and *rict-1* mutant
1234 animals fasted on standard NGM plates (150 mOsm) or high osmolarity NGM plates
1235 (300 mOsm).
1236 (C) Relative expression of str-44::T2A-mNeonGreen in *rict-1, daf-2, rict-1;daf-2, daf-16,* and
1237 *rict-1;daf-16* mutants compared to wild-type controls. (D) Schematic depicting the parallel
1238 pathways that converge on AWA to modulate *str-44* expression, which in turn modulates food-
1239 seeking behavior.
1240
1241
1242 For (A-C), each condition measured in two independent sessions. ****$p < 0.0001$, ***$p < 0.001$,
1243 **$p < 0.01$, *$p < 0.05$ by two-tailed t-test with Bonferroni correction. Colored dots represent
1244 from individual cells, black dots represent median values, shaded area shows kernel density
1245 estimation for the data.

1246

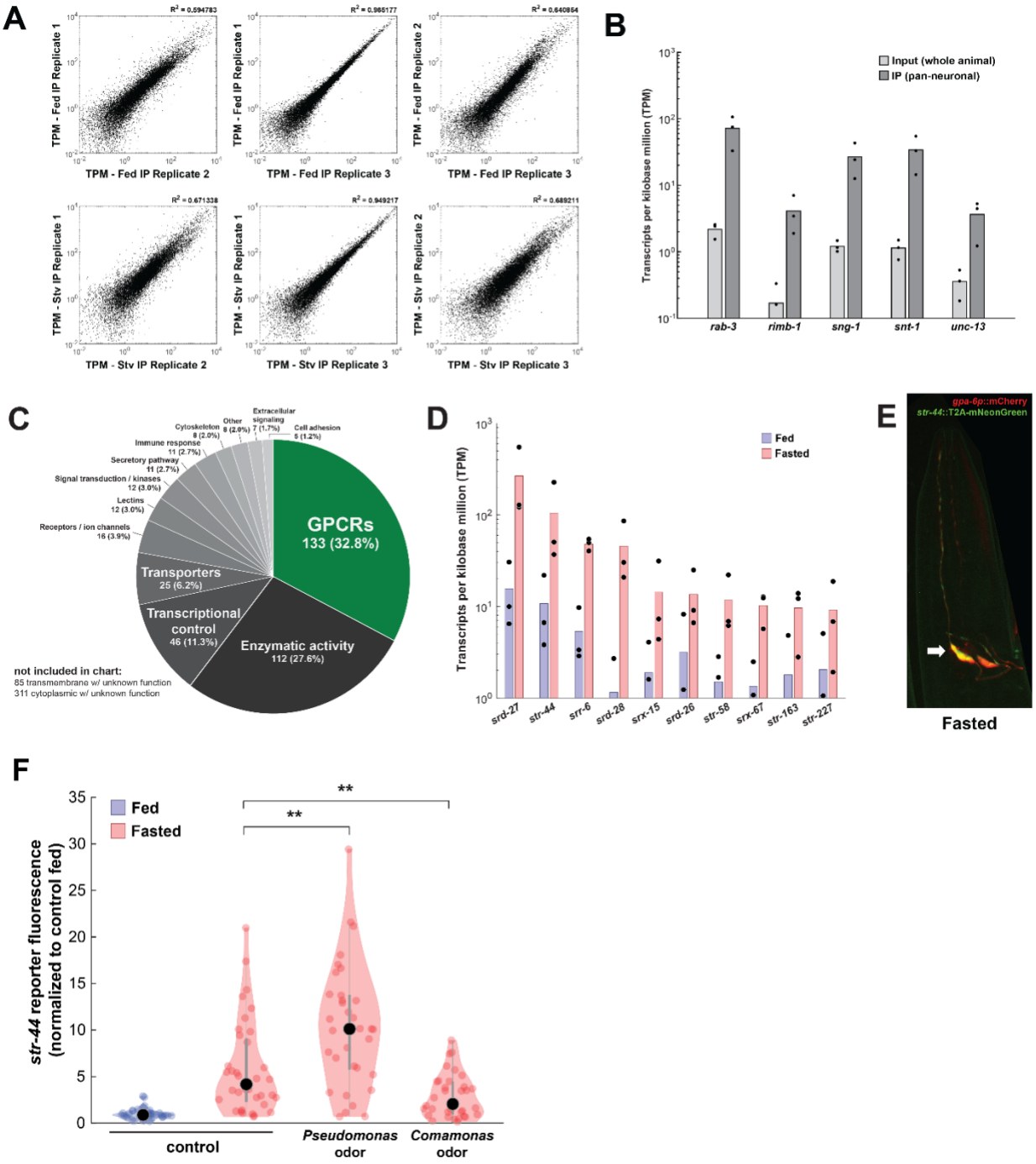

1247 **Figure 1 - supplement 1**

1248 **Figure 1—figure supplement 1.**
1249 (A) Correlation of expression values (shown as transcripts per kilobase million (TPM)) between
1250 each of three biological replicates of pan-neural ribotagging from well-fed (top row) and fasted
1251 (bottom row) animals.
1252 (B) Transcript levels of known pan-neuronal genes in input and pan-neural ribotagging samples,
1253 indicating enrichment of neuronal mRNAs in ribotag transcripts.
1254 (C) Pie chart showing gene ontology for genes upregulated by fasting. There is a significant
1255 enrichment of chemosensory GPCRs compared to the overall prevalence of chemosensory
1256 GPCRs across the genome ($p < 0.001$, Fisher Exact Test).
1257 (D) Expression levels (as transcripts per kilobase million) for the top ten fasting-upregulated
1258 chemoreceptors predicted to be expressed in AWA. Dots: measurement in each of three
1259 biological replicates; bars: means of replicates. Replicates not shown had no detected expression
1260 for that gene.
1261 (E) Co-expression of the AWA marker *gpa-6*p::mCherry (red) with the *str-44*::T2A-
1262 mNeonGreen (green) reporter in a fasted animal. Arrow indicates one of the two AWA neurons;
1263 *str-44* is expressed in both left and right AWA neurons.
1264 (F) Relative expression of *str-44*::T2A-mNeonGreen in animals that were well-fed, fasted for
1265 three hours, or fasted for three hours in the presence of the inaccessible odors from the indicated
1266 bacterial species on the lid of the plate. *str-44*::mNeonGreen reporter expression was increased
1267 significantly compared to *E. coli* OP50 controls when animals were fed DA1877 or PA14
1268 (Figure 1F). These changes could be due to differences in sensory cues and/or metabolic
1269 contents of these bacteria. To distinguish between these possibilities, we compared those results
1270 to conditions where the odors from these bacteria were present, but the bacteria could not be
1271 consumed, shown here. As is shown, adding PA14 odors on the lid of the plate increased *str-44*
1272 reporter fluorescence beyond the levels in fasted controls, similar to when animals consumed
1273 PA14. This suggests that PA14 volatiles alone can increase *str-44* expression. Adding DA1877
1274 odors on the lid of the plate decreased *str-44* expression compared to animals fasted without any
1275 bacterial odors. This result contrasts with our finding that edible DA1877 increased *str-44*
1276 expression (Figure 1F) and suggests that DA1877 odors and metabolic contents drive opposing
1277 effects on *str-44* expression, with odors decreasing *str-44* expression and metabolic contents
1278 increasing it. $^{**}p < 0.01$ by two-tailed t-test with Bonferroni correction. Colored dots represent
1279 individual cells, black dots represent median values, shaded area shows kernel density estimation
1280 for the data.

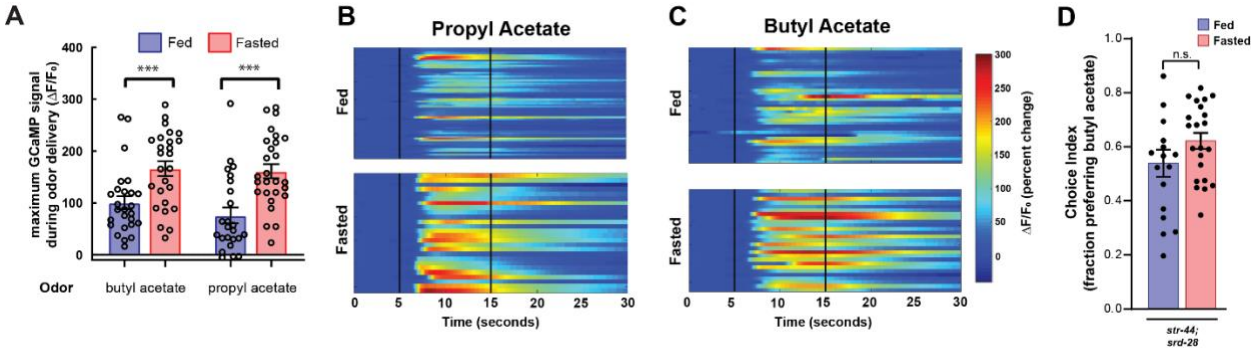

Figure 2 - supplement 1

Figure 2—figure supplement 1.

(A) Quantification of odor-induced AWA calcium imaging data from Figures 2C and 2D. Dots show maximum GCaMP signal from each animal; bars show mean ± SEM.. ***p< 0.001, one-way ANOVA with Bonferroni's Multiple Comparisons test.

(B) AWA calcium responses to propyl acetate in individual fed (top) and fasted (bottom) animals. Black vertical lines show stimulus onset and offset. Average traces are shown in Figure 2C.

(C) AWA calcium responses to butyl acetate in individual fed (top) and fasted (bottom) animals. Black vertical lines show stimulus onset and offset. Average traces are shown in Figure 2D.

(D) Food choice behavior in *str-44;srd-28* mutant animals showing fraction of animals that chose the food lawn with a spot of 1:10,000 butyl acetate. Bars show mean ± SEM. n > 15 plates per odor over two independent sessions, each with 40-200 animals.

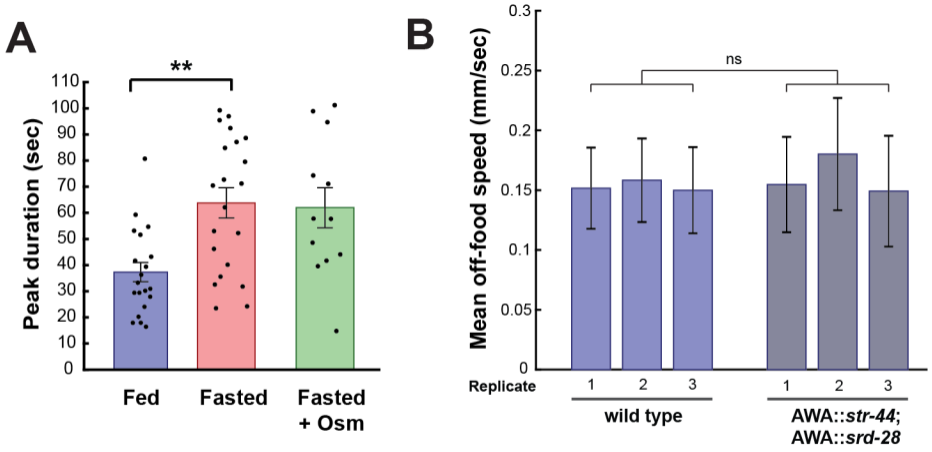

Figure 3 - supplement 1

Figure 3—figure supplement 1.
(A) Duration of each GCaMP peak in fed animals, fasted animals, and animals fasted in the presence of osmotic stress (300 mOsm). Bars show mean ± SEM. **p < 0.01, t-test with Bonferroni correction.
(B) Mean off-food locomotion in fed wild-type animals and fed animals overexpressing *str-44* and *srd-28* chemoreceptors in AWA (*gpa-6p*). Bars show mean ± s.d. Three biological replicates are shown. There is no significant difference between experimental groups.

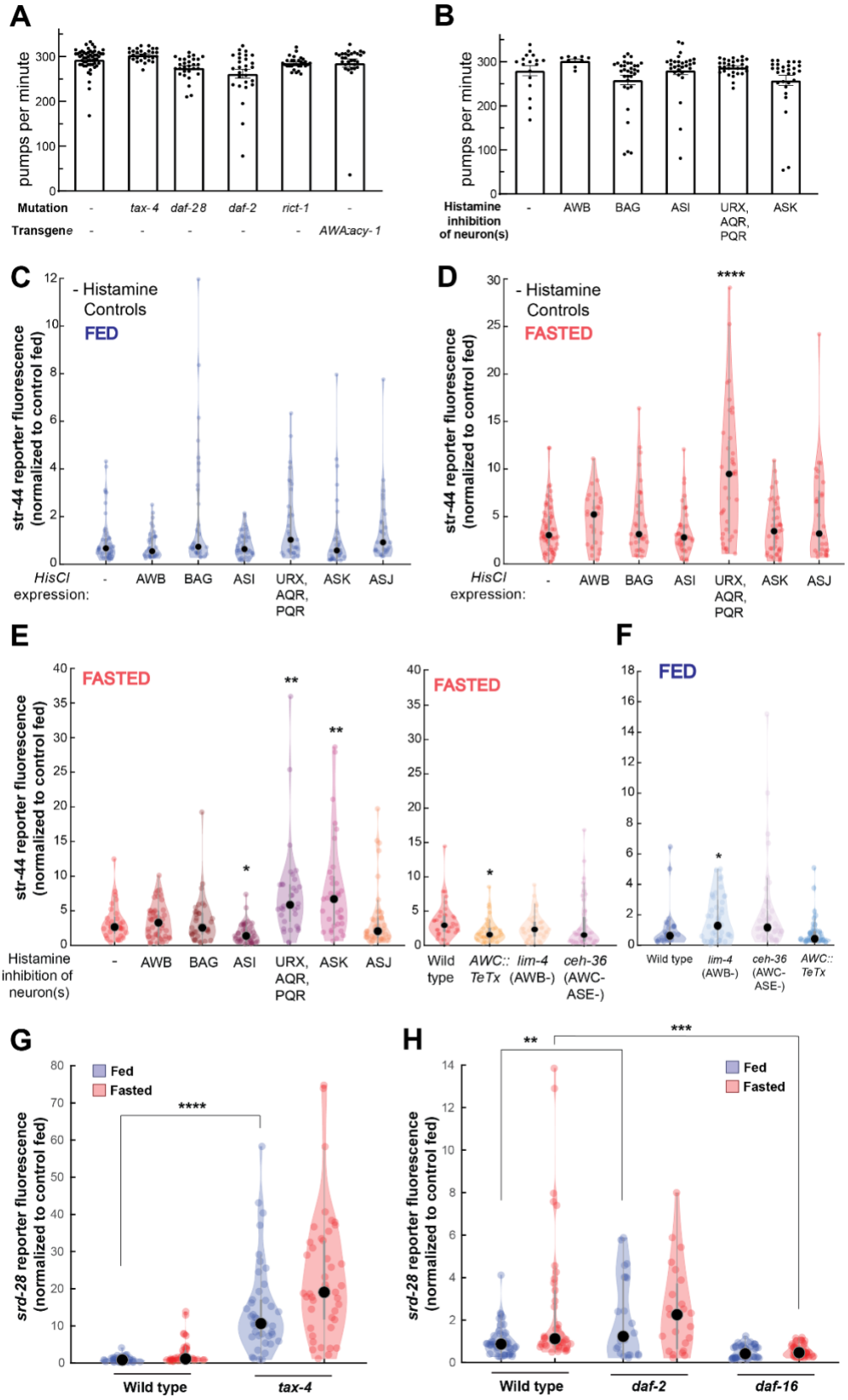

Figure 4 - supplement 1

Figure 4—figure supplement 1.
(A) Pharyngeal pumps per minute for mutants and transgenic strains that show enriched levels of *str-44*::T2A-mNeonGreen in the fed state. No significant differences observed, suggesting that the increased *str-44* expression in fed animals is not due to a reduction in feeding. Bars show mean ± SEM.
(B) Pharyngeal pumps per minute for HisCl-silencing lines after one hour on histamine plates with OP50. No significant differences observed, suggesting that the increased *str-44* expression in fed animals is not due to a reduction in feeding. Bars show mean ± SEM. (C) Histamine-absent fed controls: relative expression of *str-44*::T2A-mNeonGreen for HisCl-silencing lines for AWB (*str-1*p::HisCl1), BAG (*gcy-33*p::HisCl1), ASI (*srg-47*p::HisCl1), URX, AQR, PQR (*gcy-36*p::HisCl), ASK (*sra-9*p::HisCl1), ASJ (*srh-11*p::HisCl1) on NGM plates without histamine added. No significant differences observed.
(D) Histamine-absent starved controls: relative expression of *str-44*::T2A-mNeonGreen for HisCl-silencing lines for AWB (*str-1*p::HisCl1), BAG (*gcy-33*p::HisCl1), ASI (*srg-47*p::HisCl1), URX, AQR, PQR (*gcy-36*p::HisCl), ASK (*sra-9*p::HisCl1), ASJ (*srh-11*p::HisCl1) on NGM plates without histamine added. Note that there is a significant increase in the URX/AQR/PQR::HisCl1 line in these starved animals, indicating that the increase detected in the presence of histamine (panel E of this figure) is not actually due to neural silencing.
(E) Left: *str-44*::T2A-mNeonGreen expression following three-hour histamine-induced inhibition of sensory neurons while fasting. Histamine-gated chloride channel (HisCl1) transgenes expressed with cell-specific promoters detailed in panel (d) of this figure. Note that there is a significant increase in the URX/AQR/PQR::HisCl1 line in histamine-absent starved controls (panel D of this figure), indicating that the increase detected here in the presence of histamine is not actually due to neural silencing. Right: *str-44*::T2A-mNeonGreen expression following genetic ablation of sensory neurons (AWB: *lim-4(ky403)*; AWC/ASE*: ceh-36(ks86)*) or synaptic silencing by tetanus toxin light chain (AWC::TeTx) in fasted animals.
(F) *str-44*::T2A-mNeonGreen expression following genetic ablation of sensory neurons (AWB: *lim-4(ky403)*; AWC/ASE: *ceh-36(ks86)*) or synaptic silencing by tetanus toxin light chain (AWC::TeTx) in well-fed animals.
(G) *srd-28*::T2A-mNeonGreen expression in *tax-4(p678)* mutants compared to wild-type controls.
(H) *srd-28*::T2A-mNeonGreen expression in *daf-2(m41)* and *daf-16(mu86)* mutants compared to wild-type controls.

For (C-H), each condition measured in two independent sessions. ****$p < 0.0001$, ***$p < 0.001$, **$p < 0.01$, *$p < 0.05$ by two-tailed t-test with Bonferroni correction. Colored dots represent from individual cells, black dots represent median values, shaded area shows kernel density estimation for the data.

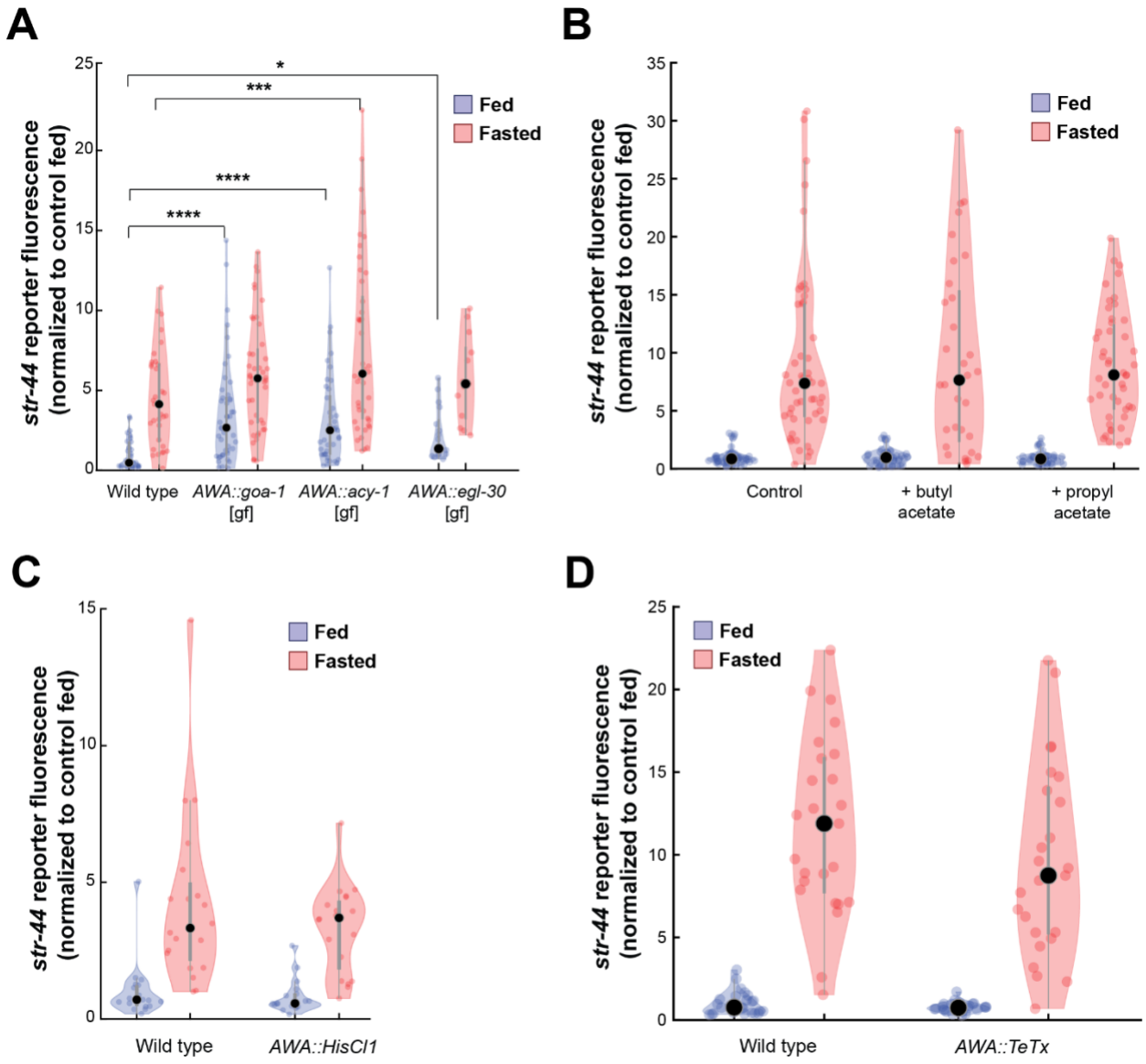

Figure 4 - supplement 2

Figure 4—figure supplement 2.
(A) Relative expression of *str-44*::T2A-mNeonGreen in animals expressing the indicated constitutively-active G proteins in AWA (*gpa-6*p). ****p < 0.0001, ***p < 0.001, *p<.05 by two-tailed t-test with Bonferroni correction.
(B) Relative expression of *str-44*::T2A-mNeonGreen in animals exposed to the putative *str-44* ligands butyl acetate and propyl acetate during feeding or fasting (1:100 dilution on lid of plate). There is no significant difference between odor and non-odor conditions.
(C) Histamine-absent controls: relative expression of *str-44*::T2A-mNeonGreen for AWA silencing line (*gpa-6*p::HisCl1) on NGM plate lacking histamine. There is no significant difference between genotypes in this control (histamine-absent) condition.

1357 (D) Relative expression of *str-44*::T2A-mNeonGreen in animals with synaptic silencing of AWA
1358 (*gpa-6*p::TeTx). There is no significant difference between genotypes.
1359
1360 For (A-D), each condition measured in two independent sessions. Colored dots represent from
1361 individual cells, black dots represent median values, shaded area shows kernel density estimation
1362 for the data.

1363

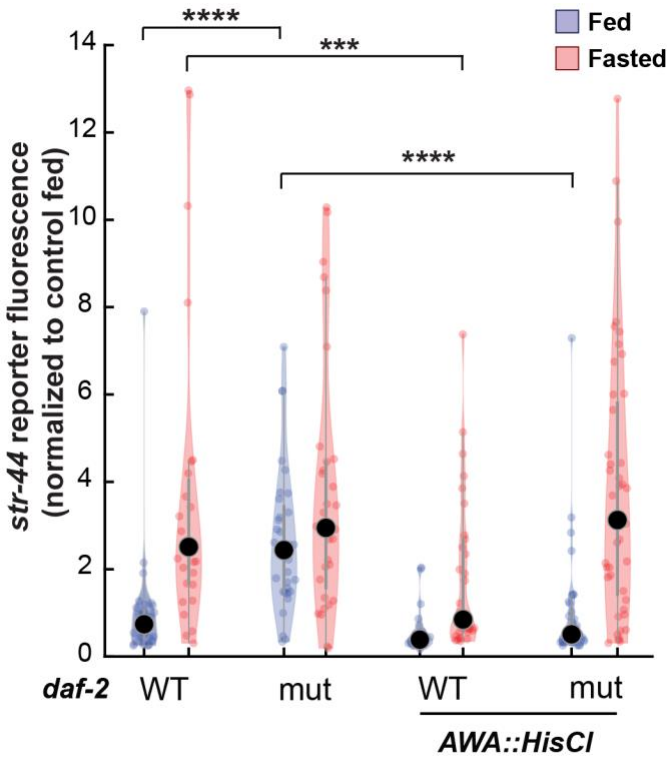

1364
1365
1366 **Figure 6—figure supplement 1.**
1367 Relative expression of *str-44*::T2A-mNeonGreen in *daf-2, AWA::HisCl,* and *AWA::HisCl;daf-*
1368 *2* mutants compared to wild-type control. Note that these animals were all in the presence of
1369 histamine.
1370
1371 Each condition measured in two independent sessions. ****$p < 0.0001$, ***$p < 0.001$ by two-
1372 tailed t-test with Bonferroni correction. Colored dots represent from individual cells, black dots
1373 represent median values, shaded area shows kernel density estimation for the data.

1374 **Legends for Supplementary Files**
1375
1376 **Supplementary File 1. List of neuronal genes whose expression is altered by fasting.**
1377 Table of genes that are upregulated or downregulated in neurons in fasted animals. Transcripts
1378 from neuronal ribotagging biological replicates (three per condition, fed versus fasted) were
1379 mapped to the *C. elegans* genome (WBcel235) with kallisto then analyzed for differential
1380 expression of annotated genes with sleuth. Sleuth generated a gene-level model fit to ribotagged
1381 vs. input and fed vs. fasted conditions. A Wald test was then applied to generate a beta statistic
1382 (b), which approximates to the log2 fold-change in expression between the fed and starved
1383 conditions. Genes were included if b>2 (upregulated in fasted, 802 genes) or b<-2
1384 (downregulated in fasted, 647 genes).